Kataoka *et al. Earth, Planets and Space (2018) 70:113*
https://doi.org/10.1186/s40623-018-0873-x

Earth, Planets and Space

FULL PAPER

Open Access

Lahar characteristics as a function of triggering mechanism at a seasonally snow-clad volcano: contrasting lahars following the 2014 phreatic eruption of Ontake Volcano, Japan

Kyoko S. Kataoka[1*], Takane Matsumoto[1], Takeshi Saito[2], Katsuhisa Kawashima[1], Yoshitaka Nagahashi[3], Tsutomu Iyobe[4], Akihiko Sasaki[5,6] and Keisuke Suzuki[5]

Abstract

In association with the September 2014 phreatic eruption (VEI 1–2) at Ontake Volcano, a syn-eruptive and two post-eruptive lahars occurred in the Akagawa–Nigorigawa River, southern flank of the volcano. The present contribution describes and discusses the contrasting features of the two post-eruptive lahars, which caused a major impact on downstream river morphology, and re-examines the description of the syn-eruptive lahar in the previous study. The first post-eruptive lahar occurred 8 days after the eruption by the rainstorm (October 5, 2014, before the snowy season), and the second lahar was associated with the rain-on-snow (ROS) event on April 20, 2015, in the early spring of the snowmelt season. The October rain-triggered lahar, which can be interpreted as a cohesive debris flow, reached at least ~ 11 km downstream and left muddy matrix-rich sediments with high clay content (10–20 wt% of clay in matrix). The lahar deposits contain hydrothermally altered rock fragments, sulfide/sulfate minerals, and clay minerals and show extremely high total sulfur content (10–14 wt%) in matrix part, indicating source material from the September phreatic eruption deposits. The presence of "rain-triggered" clay-rich lahar and deposits originating from a single small phreatic eruption is important because usually such clay-rich lahars are known to occur in association with large-scale sector collapse and debris avalanches. The April ROS-triggered lahar was caused by the heavy rain and accompanying snow melting. The lahar was dilute and partly erosional and evolved into hyperconcentrated flow, which left fines-depleted sandy and gravelly deposits. Despite these lahars that originated from the same volcanic source and occurring within a 7-month period, the flow and resulting depositional characteristics are totally different. These different types of lahars after a single eruptive event need different simulations and mitigation of lahar hazards with timing (season) of the lahar onset. In comparison with rainfall intensity, snow-melting rate, and the contrasting lahars occurred in 2014/2015, it is postulated that the generation, size, and types of lahars can vary with the timing of eruption, whether it happens during the pre-snow season, snow season, or rainy season.

Keywords: Ontake Volcano, 2014 eruption, Phreatic eruption, Clay-rich lahar, Rain-on-snow, Cohesive debris flow

*Correspondence: kataoka@gs.niigata-u.ac.jp
[1] Research Institute for Natural Hazards and Disaster Recovery, Niigata University, Ikarashi 2-8050, Nishi-ku, Niigata 950-2181, Japan
Full list of author information is available at the end of the article

Introduction

On September 27, 2014, Ontake Volcano in central Japan confronted mountaineers with an unpredicted small-scale phreatic eruption (VEI 1–2: Maeno et al. 2016) and caused 63 fatalities (including 5 missing) at the summit. Studies about the eruption and the tragedy have addressed the processes and mechanism of the eruption itself (e.g., Oikawa et al. 2016). Also, further concerns and interests immediately after the eruption were about future eruptions and their prediction: whether the eruption would evolve into magmatic explosive phase. However, there was another concern for lahar hazards with snow/ice meltwater (Major and Newhall 1989; Pierson et al. 1990; Manville et al. 2000; Waythomas 2014) such at the seasonally snow-clad Ontake Volcano. Further eruptions could trigger lahars through rapid snowmelt by hot pyroclastic density currents. Even without a new eruption, lahars remobilizing the primary September eruption deposits in upslope areas could be triggered later by heavy rain or by warm rainstorm on winter snowpack. In addition, an earthquake-triggered lahar is always a potential hazard in this region, as evidenced by the lahar triggered during the Naganoken-Seibu earthquake on September 14, 1984 (Matsuda and Ariyama 1985; Endo et al. 1989), which initiated as flank collapse of southern part of the edifice. The resulting lahar in the Denjogawa and Nigorigawa Rivers (Fig. 1a) and other landslides caused 29 fatalities. Lahars and other sediment-laden flows are serious hazards because they can cause rapid aggradation and widening of rivers from proximal to distal areas of volcanoes, inundate communities, and destroy infrastructure (Smith 1991; Newhall and Punongbayan 1996; Kataoka et al. 2009; Pierson and Major 2014).

This paper focuses on three lahars generated at Ontake Volcano within a 7-month period, each triggered by a different mechanism: a phreatic eruption, heavy rainfall, and rain-on-snow event (hereafter ROS for "rain-on-snow": Kattelmann 1985, 1997; Sui and Koehler 2001; Pradhanang et al. 2013). This paper further highlights that at Ontake Volcano, the generation, size, and types of lahars are dependent, in part, on the timing and type of eruption with respect to the presence of seasonal snowpack.

Background and settings

Historical and prehistorical eruptions of Ontake Volcano

Ontake Volcano (3067 m a.s.l. (above sea level), at summit Kengamine peak; 35°53′ 34″N, 137°28′49″E) is located on Honshu Island at the border of Nagano and Gifu Prefectures (Fig. 1). During the Holocene epoch, before the 2014 eruption, Ontake Volcano has erupted at least 21 times; most have been phreatic and three have occurred within the last 50 years. The first recorded (witnessed) historical eruption at Ontake was a phreatic eruption which occurred on October 28, 1979, from vents in Jigokudani and Haccho-tarumi (e.g., Soya et al. 1980). After the 1979 eruption, small-scale phreatic eruptions again occurred in May 1991 and March 2007 from Haccho-tarumi crater and resulted in ashfall deposition nearby the vent only. Oikawa et al. (2014) reported the presence of at least 13 phreatic eruptions during the last 7500 years before the 1979 eruption and 5 magmatic eruptions during the Holocene. Since the traces of small-scale eruptions including phreatic eruptions in geological records are limited, the eruptive records and associated lahar history of Ontake Volcano still need to be examined in detail.

The September 2014 eruption and a syn-eruptive lahar

On September 27, 2014 (11:52 a.m. Japan time), Ontake Volcano erupted suddenly with a very short precursor of tremor and edifice tilting that began 11 min before the eruption (Oikawa et al. 2014; Maeno et al. 2016). The active eruptive vents were in Jigokudani valley (Fig. 1a) with the eruptive column reaching ~ 7.8 (or 5) km high above the vents (Sato et al. 2016). The 2014 eruption included low-temperature pyroclastic density currents induced by the collapse of the volcanic plume that rose up to 300 m above the vents. The currents mainly flowed on the southern and western slopes of the volcano (Yamamoto 2014; Maeno et al. 2016) although the actual thickness of deposits confined to valleys still remains unknown. The eruption was phreatic without any juvenile materials. The ejecta consist of fragmented gray andesite and altered andesite with sulfide and sulfate minerals (Maeno et al. 2016; Minami et al. 2016). The ashfall distribution is more extensive than that of the 1979 eruption

(See figure on next page.)

Fig. 1 **a** Index map showing Mt. Ontake (Ontake Volcano) and river systems in the southern slope. Isopach of fallout and distribution of pyroclastic density currents of the 2014 eruption are after Oikawa et al. (2014) and Takarada et al. (2016). These isopach maps are based on the survey points mostly situated at the eastern, northern, and western flanks of the volcano, and very few from the southern part of medial-distal areas. Wire sensors were set at two localities in the Nigorigawa River by the Ministry of Agriculture, Forestry and Fisheries (MAFF) and the Ministry of Land, Infrastructure, Transport and Tourism (MLIT). Published topographical map and DEM (original data from the Geospatial Information Authority of Japan) were processed by Kashmir 3D. **b** Distribution of the October 2014 lahar (cohesive debris flow) deposits and outcrop localities (see also in **a**). Mapping is based on the authors' ground survey and captured aerial photo-images taken 2 days after the lahar (Courtesy to Google Earth). **c** Longitudinal profiles of the Akagawa and Nigorigawa Rivers and distribution of the October 2014 lahar deposits and installed wire sensors

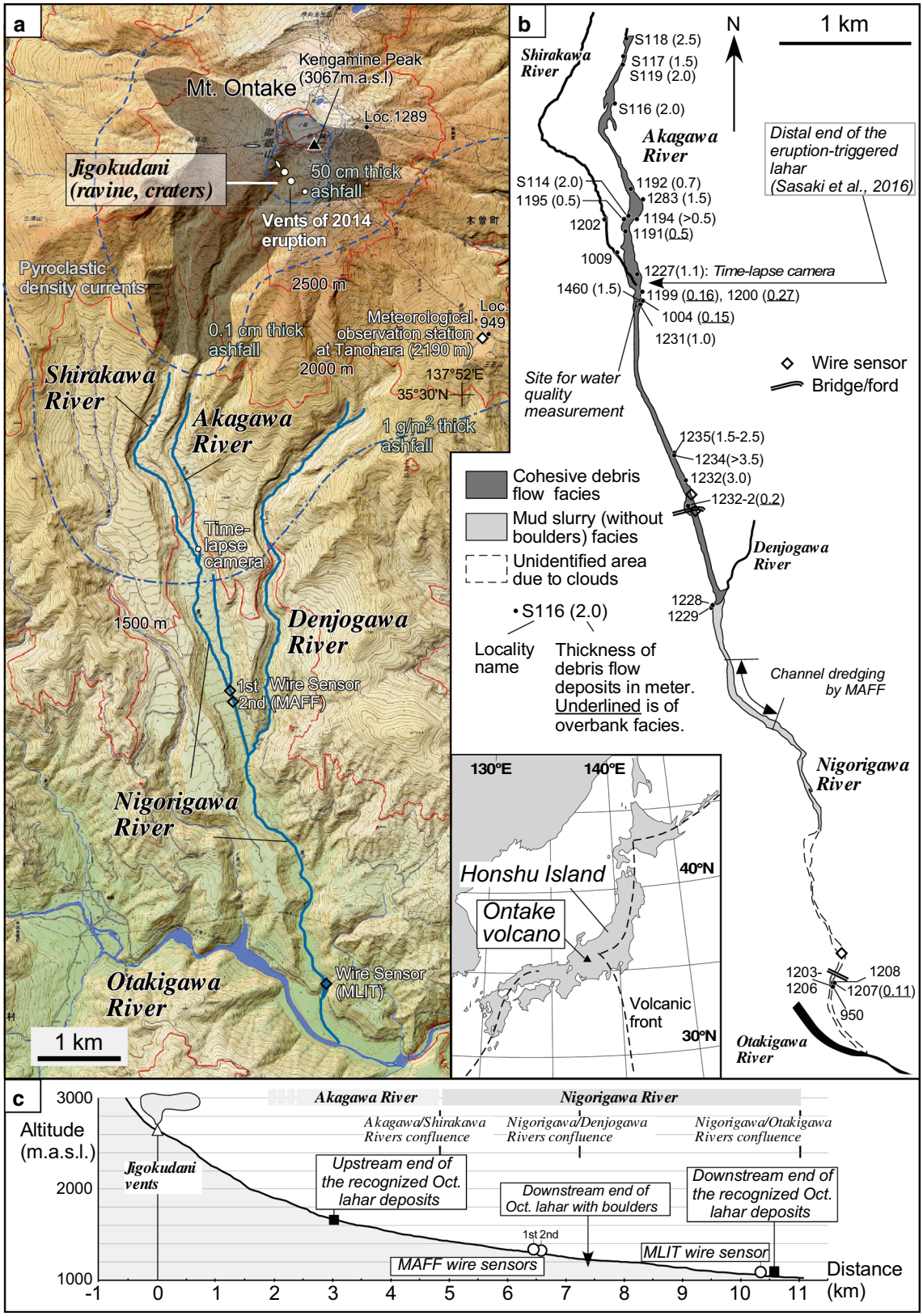
a
Kengamine Peak (3067m.a.s.l)
Mt. Ontake
Loc.1289
Jigokudani (ravine, craters)
50 cm thick ashfall
Vents of 2014 eruption
Pyroclastic density currents
2500 m
0.1 cm thick ashfall
Meteorological observation station at Tanohara (2190 m)
Loc. 949
2000 m
137°52'E
35°30'N
1 g/m2 thick ashfall
Shirakawa River
Akagawa River
Time-lapse camera
1500 m
Denjogawa River
1st Wire Sensor
2nd (MAFF)
Nigorigawa River
Wire Sensor (MLIT)
Otakigawa River
1 km
b
N
1 km
Shirakawa River
S118 (2.5)
S117 (1.5)
S119 (2.0)
S116 (2.0)
Akagawa River
Distal end of the eruption-triggered lahar (Sasaki et al., 2016)
S114 (2.0)
1195 (0.5)
1202
1192 (0.7)
1283 (1.5)
1194 (>0.5)
1191(0.5)
1009
1227(1.1): Time-lapse camera
1460 (1.5)
1199 (0.16), 1200 (0.27)
1004 (0.15)
1231(1.0)
Site for water quality measurement
Wire sensor
Bridge/ford
1235(1.5-2.5)
1234(>3.5)
1232(3.0)
1232-2(0.2)
Cohesive debris flow facies
Mud slurry (without boulders) facies
Unidentified area due to clouds
Denjogawa River
1228
1229
•S116 (2.0)
Locality name
Thickness of debris flow deposits in meter. Underlined is of overbank facies.
Channel dredging by MAFF
Nigorigawa River
130°E
140°E
Honshu Island
40°N
Ontake volcano
Volcanic front
30°N
1203-1206
1208
1207(0.11)
950
Otakigawa River
c
Altitude (m.a.s.l.)
3000
2000
1000
Akagawa River
Nigorigawa River
Akagawa/Shirakawa Rivers confluence
Nigorigawa/Denjogawa Rivers confluence
Nigorigawa/Otakigawa Rivers confluence
Jigokudani vents
Upstream end of the recognized Oct. lahar deposits
Downstream end of Oct. lahar with boulders
Downstream end of the recognized Oct. lahar deposits
1st 2nd
MAFF wire sensors
MLIT wire sensor
-1
0
1
2
3
4
5
6
7
8
9
10
11
Distance (km)

(Oikawa et al. 2014; Takarada et al. 2016). The volume of eruption deposits is estimated as $0.7–1.3 \times 10^6$ m^3, suggesting a very small-scale VEI 1–2 eruption (Maeno et al. 2016). Most of the ashfall deposits are distributed east of the vents because of the prevailing westerly winds (Fig. 1a: Oikawa et al. 2014; Maeno et al. 2016; Takarada et al. 2016). Aerial photographs suggest a thin layer of ash mantles the southern slope (Oikawa et al. 2014; Maeno et al. 2016; Takarada et al. 2016). Fumaroles have been commonly observed around vents in the Jigokudani valley before and after the eruption.

On the syn-eruptive lahar, aerial photographs taken around the Jigokudani vents approximately 2–4 h and 1 day after the eruption (Kaneko et al. 2016) indicate that a relatively small of volume of mud slurry (mudflows) was expelled from the vents. Sasaki et al. (2016) reported the distribution of mudflow deposits from the vents to 5 km downstream in the Akagawa River, southern slope of the volcano, on the basis of aerial photographs taken 1 day after the eruption (Fig. 1b). They interpreted from the aerial photographs that the mudflow expelled from the vents directly and continuously travelled 5 km to the Akagawa River as a lahar. However, uncertainty about these observations arises because the interpretation was not supported by any field evidence. Alternative possibility for the origin of the syn-eruptive lahar, such as transformation of pyroclastic density currents, has not been discussed by the previous studies.

Nigorigawa River system and regional climate

The Nigorigawa River system consists of two main tributaries in the upstream area; Akagawa River and Shirakawa River (Fig. 1a). The two rivers run parallel on the volcanic slope, although only the Akagawa River catchment holds active Jigokudani vents in the head of the river valley.

Ontake Volcano is under a temperate climatic condition with seasonal snow cover from November to May around the top of the mountain. The annual maximum snow depth, the annual mean air temperature, and the annual precipitation are 76 cm, 7.4 °C, and 2065 mm, respectively, at the Kaidakogen weather station (1130 m a.s.l.), located ~ 11 km northeast of the summit of the volcano and operated by Japan Meteorological Agency for 30 years from 1981 to 2010. In order to understand the amount of water input to the Nigorigawa River catchment, the present authors carried out meteorological observations at Tanohara (on the southeastern slope, 2190 m a.s.l.; Fig. 1a), which is quite close to a precipitation gauge operated by Japan Meteorological Agency. Obtained rainfall data and rate of snowmelt are based on the measurements of energy balance components at the snow surface (e.g., DeWalle and Rango 2008) during the winters of 2014/2015 and 2015/2016 (Fig. 2).

After the eruption on September 27, two typhoon events caused > 100 mm of cumulative rainfall on October 5 and 13, 2014, before any snowpack had accumulated (Fig. 2a). Snow started to accumulate at the end of November, with a maximum thickness of 2 m by the middle of March, which was completely melted on April 20, 2015, at the Tanohara observation site (Fig. 2). At least three ROS events resulting in major stage changes during the snow-melting season were observed in records of a time-lapse camera at the Akagawa River set by the authors (Fig. 2a and the supplementary movie file as in Additional file 1). Wire sensors, which were set up for a debris flow alert in the Nigorigawa River system (Fig. 1), were activated only by two lahar events on October 5, 2014 (second rainstorm after the eruption), and on April 20, 2015 (the last ROS). This means that the rest of heavy rainfall and ROS events caused no or minimal mass transport to have resulted in any significant geomorphological changes to the river during the period. After April 20, 2015, to the end of observation period in 2016, rainstorms as well as ROS conditions were observed, but major lahars did not occur. Wire sensors did not detect any lahars after the ROS-triggered lahar on April 20, 2015.

Methodology

Several analyses, in the field and in laboratories, were performed in this study. Analyses for this study consisted of (1) geological and sedimentological surveys to identify lahar deposits, (2) river image capturing by a time-lapse camera over a 13-month period from November 2014 to November 2015, and (3) grainsize of lahar deposits, and (4) XRF (X-ray fluorescence) and

(See figure on next page.)

Fig. 2 **a** Timelines of the eruption and lahars with temporal variations in the daily rainfall, daily rate of snowmelt, and snow depth at Tanohara (2190 m a.s.l.: Fig. 1a). The October 2014 lahar was caused by the second rainstorm event after the eruption, whereas the April ROS-induced lahar occurred due to the most intensive water supply which was ~ 400 mm at the end of the snowmelt season. **b** Hourly rainfall intensity at Tanohara on October 5–6, 2014 (left), and hourly rainfall + snowmelt intensity on April 20–21, 2015 (right). **c** Daily water input and snow depth at Tanohara from September 27, 2014, to September 25, 2016 (24 months)

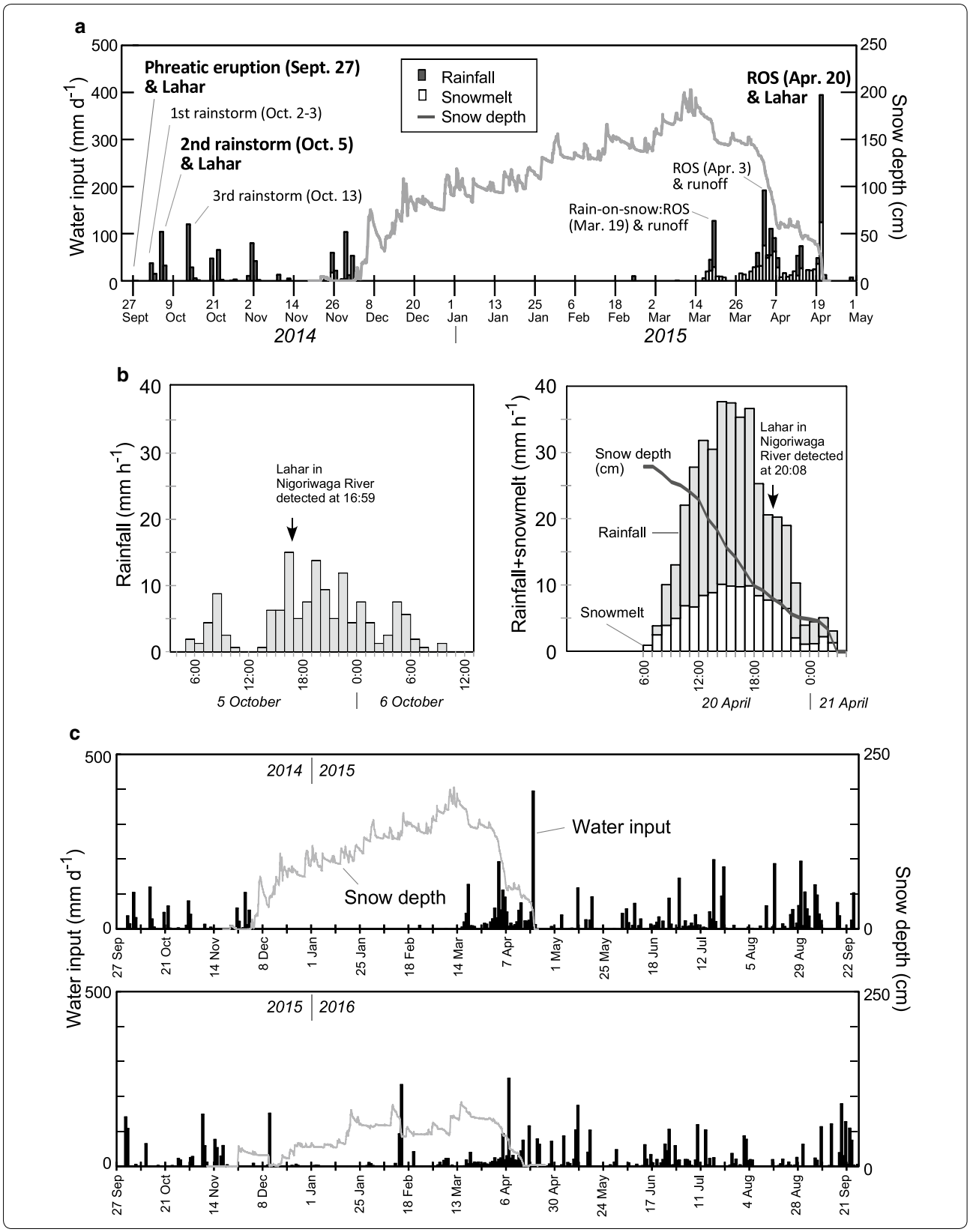
a
Water input (mm d-1)
Snow depth (cm)
Rainfall
Snowmelt
Snow depth
Phreatic eruption (Sept. 27) & Lahar
1st rainstorm (Oct. 2-3)
2nd rainstorm (Oct. 5) & Lahar
3rd rainstorm (Oct. 13)
ROS (Apr. 20) & Lahar
ROS (Apr. 3) & runoff
Rain-on-snow:ROS (Mar. 19) & runoff
27 Sept
9 Oct
21 Oct
2 Nov
14 Nov
26 Nov
8 Dec
20 Dec
1 Jan
13 Jan
25 Jan
6 Feb
18 Feb
2 Mar
14 Mar
26 Mar
7 Apr
19 Apr
1 May
2014
2015
b
Rainfall (mm h-1)
Lahar in Nigoriwaga River detected at 16:59
5 October
6 October
Rainfall+snowmelt (mm h-1)
Snow depth (cm)
Rainfall
Snowmelt
Lahar in Nigoriwaga River detected at 20:08
20 April
21 April
c
Water input (mm d-1)
Snow depth (cm)
2014 | 2015
Water input
Snow depth
27 Sep
21 Oct
14 Nov
8 Dec
1 Jan
25 Jan
18 Feb
14 Mar
7 Apr
1 May
25 May
18 Jun
12 Jul
5 Aug
29 Aug
22 Sep
2015 | 2016
27 Sep
21 Oct
14 Nov
8 Dec
1 Jan
25 Jan
18 Feb
13 Mar
6 Apr
30 Apr
24 May
17 Jun
11 Jul
4 Aug
28 Aug
21 Sep

XRD (X-ray diffraction) analyses of lahar component particles.

Geological and sedimentological surveys to identify lahar deposits

Distribution, thickness, sedimentary facies, and lithological characteristics of lahar deposits in the Akagawa–Nigorigawa River valley were described in the field. Regular monthly to bimonthly field survey after the eruption enabled the identification of new lahar deposits with timing of their emplacement, and to document the drastic geomorphic changes of the Akagawa–Nigorigawa River over the period of the study.

Image capturing of river water discharge

Since November 2014, the authors deployed an automatic camera (time-lapse camera) in the Akagawa River at 4.7 km downstream from the vents (Fig. 1: nearby Loc. 1227 at the check dam) to observe changes in river discharge, turbidity, and geomorphology (the supplementary movie file in Additional file 1). The camera captures one shot every 10 min during daytime.

Grainsize analysis

Samples for grainsize analysis were collected only for those materials that are finer than approximately 10 cm in size. Lahar deposits contain larger clasts (tens of cm to 1 m in size); therefore, the samples represent predominantly matrix fraction of the whole sediments. Sample quantities of about 200–1000 g of dry weight for meter-thick deposits and less than 100 g for decimeter- to centimeter-thick deposits were collected. Sandy and gravelly samples were dry-sieved and separated by grain fractions in a phi scale, whereas muddy sediments were wet-sieved after dried samples (weighted) were soaked in water medium, and were separated by a sieve with a mesh size of 63 μm. Grains larger than 63 μm (sand and gravel) were again dry-sieved in a phi scale. Petrography of sieved samples (1/4–1/8 mm fraction) was carried out under binocular and petrographic microscopes. Grainsize for smaller than 63 μm (i.e., mud fraction) was examined by a laser grainsize analyzer, Malvern Mastersizer 3000 at Niigata University. Five portions were randomly collected from each sample, and each portion was measured five times (therefore a total 25 runs for one sample) with duration of 15 s for each run. Averages of the total runs represent grainsize for each sample.

XRF analysis

XRF analyses for powder-pressed pellets of bulk samples of ashfall, lahar, and pre-eruptive fluvial deposits were performed with Rigaku RIX1000 and RIX2000 at Fukushima University. The accelerating voltage and tube current were 50 kV and 50 mA. Data for major element and total sulfur (as SO_3) content are semiquantitative by the FP (fundamental parameter) method with a standardless technique (Takase and Nagahashi 2007). Sulfur content in each sample is high enough to discuss comparison among individual samples. Trace element contents were quantified by the calibration curve method (Nagahashi and Nakazawa 2016).

XRD analysis

For muddy sediments, XRD analysis (by Rigaku Ultima IV at Niigata University) was performed to understand the mineral composition and to discuss the origin and relation of the 2014 phreatic eruption with lahars. Samples were prepared for bulk analysis (powdered) and for fine fraction (clay mineral) analysis after separation by hydraulic settling and centrifuge. Samples for clay mineral analysis were measured as (1) oriented and (2) heated at 400 and 550 °C conditions. Some samples were treated with ethylene glycol and HCl to identify the minerals overlapping in certain cell parameters. Measurement conditions were of CuKα radiation, 40 kV and 40 mA, and scanning speed of 2° per minute.

Description of the rain-triggered lahar and deposits on October 5, 2014

Overview

The first rainstorm event after the eruption occurred on October 2–3, 2014, with total 52.5 mm precipitation (corrected value by wind velocity data) recorded on the rain gauge at Tanohara. However, this rainstorm with maximum 6.9 mm/h did not trigger a lahar. The second rainstorm associated with a typhoon (the 18th typhoon in year 2014 in Japan) was 8 days after the eruption, on October 5, and did trigger a lahar. The lahar was detected in the Nigorigawa River at 4:59 p.m. based on a wire-sensor alert system at 6.5 km from the vents (Fig. 1) deployed by the Forestry Agency at the Kiso Office (Hayashi et al. 2015, and public announcement by the Forestry Agency, Kiso Office: http://www.rinya.maff.go.jp/chubu/koho/ontakesan/pdf/141105-ontaketaiou.pdf). The wire sensor was placed at 1.0–1.4 m above the riverbed. Cumulative rainfall from early morning to 5 p.m. was 47.5 mm, and total precipitation during the day rose to 104.4 mm (Fig. 2). The peak hourly precipitation was 15 mm/h during the hour from 4 to 5 p.m. A third rainstorm on October 13–14 was again associated with a typhoon. Although heavier rainfall of total 120 mm during the day and intensive rain over 6 h (exceeding 10 mm every hour) were recorded, the rain event did not trigger a lahar.

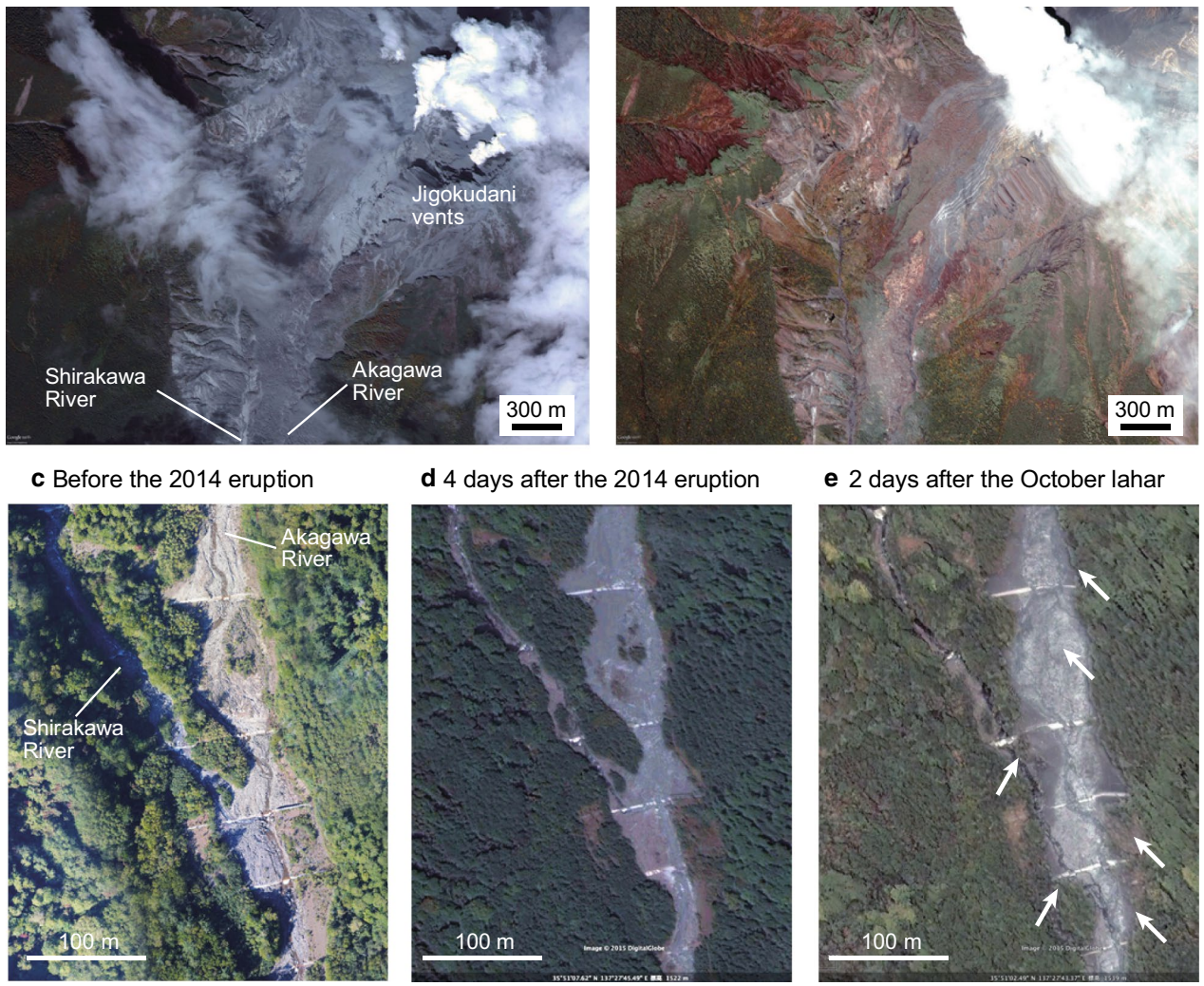

Fig. 3 Aerial photographs of the catchment of Akagawa and Shirakawa Rivers. **a** Google Earth image captured immediately after the eruption (on October 1, 2014) and **b** October 7, just 2 days after the rain-triggered lahar occurred on October 5 in the upstream and summit areas. Much of the slope-covered ashfall materials were swept away by the rainstorm. **c** Picture taken before the 2014 eruption (the area captured during August to November 2013 by the Geospatial Information Authority, Japan) of the confluence area of the Akagawa and Shirakawa Rivers (the same area in **d** and **e**). **d** Google Earth image captured on October 1. **e** Image (by Google Earth) showing the impact after the lahar (taken on October 7). Arrows indicate areas where major geomorphological changes (erosion and overbank deposition) by the lahar were identified

Aerial photo-images captured by the Geospatial Information Authority, Japan, and Google Earth images provide evidence that the first and second rainstorms and the lahar caused high degradation and deposition with major geomorphic changes on the southern flank of the edifice and in the river courses (Fig. 3). On October 1, before the rainstorms, gray areas near the vents and farther downslope indicate mantling by ash. Images of the river valley, where a pyroclastic density current descended, also show mantling by ash (Fig. 3a). Images taken 2 days after the lahar (on October 7) show extensive erosion of the ash on the southern flank, with underlying brown to reddish brown altered rock and deposits then exposed by the rain and lahar (Fig. 3b). These changes correspond with the aerial observation by Oikawa et al. (2015), in which they reported disappearance of a mound of pyroclastic deposits in the Jigokudani area after these rainstorms. The river channel in downstream areas also shows changes. Comparison of aerial photographs of the confluence area of the Akagawa and Shirakawa Rivers (Fig. 3c–e) taken in 2013 and after the 2014 eruption (on October 1 and 7) reveals major geomorphological changes (erosion of riparian forests and bars and deposition at overbank) caused by the lahar.

Table 1 Area, representative thickness, and estimated volume of the October 2014 rain-triggered lahar deposits

	Area (m^2)	Average thickness (m)	Volume (m^3)
Cohesive debris flow with boulders (from the Akagawa to the confluence of the Denjogawa River)	1.8×10^5	1.5	2.7×10^5
Mud slurry facies (from the Akagawa/Denjogawa Rivers confluence to the Otaki River)	1.4×10^5	0.11	1.5×10^4

Aerial photographs and field investigation revealed that overbank flows reached the confluence with the Shirakawa River (Fig. 1b). The lahar deposits with boulders were distributed down to the confluence of Nigorigawa and Denjogawa Rivers, and fine-grained flows travelled further downstream (Fig. 1b, c: Hayashi et al. 2015). The total volume of the October lahar deposits is roughly estimated as 2.9×10^5 m^3 (Table 1).

Deposits

The October lahar left deposits not only in the main river channel, but also spilled sediments over banks onto side terraces (Figs. 4, 5). The deposits were recognized between 3 km from the vents in Jigokudani (Loc. S118 in Fig. 1b) and the downstream end of the Nigorigawa River (10.5 km from the vents: Loc. 1207, Fig. 4i) where the larger Otakigawa River joins (Fig. 1). The gray-colored fine ash deposit (possibly derived from ash cloud of the pyroclastic density current) overlain by the lahar deposits is recognized at Loc. S118. The ash deposit mantles underlying pre-eruptive deposits.

Thickness of the lahar deposits in the Akagawa and Nigorigawa Rivers varies between 1 and 3 m for in-channel facies (Fig. 4c–e) and 0.1 and 0.5 m for overbank facies (Fig. 4g–i). In-channel facies is defined as deposits that rest directly on fluvial gravel, whereas overbank deposits overlie soil and vegetation developed on banks and terraces (Figs. 4a, 5, 6a, b). Occasionally, run-up deposits on sidewall of the valley up to 1 to 1.4 m high can be observed (Fig. 4c). Mud lines were left on trees and leaves. On the surface of deposits wrinkles and ridges formed by compression are present (Fig. 4b). Overbank deposits are identified on a sabo-dam (check dam at Loc. 1227) 3 m above its base (Fig. 5a). Facies, texture, and composition of in-channel and overbank deposits (components less than 8 mm) are usually similar in an outcrop scale (vertical and lateral), and from the proximal to distal locations, however, thickness and content of clasts larger than 8 mm decreased toward downstream (Figs. 4, 5, 6a, b). The presence of boulders in the deposits diminishes beyond the confluence with the Denjogawa River where the valley widens.

The lahar deposits are muddy matrix supported, massive, and unstratified (Fig. 4). Approximately 40 days after the lahar event (November 12, 2014), the deposits were still fluidal, i.e., wet, viscous, and swampy, but they had become hard when the authors revisited the deposits 7 months after deposition. Locally 2-cm-thick sole layers (matrix material without clasts) occupy the base of sequence. The matrix is very poorly to extremely poorly sorted ($\sigma_I = 3$ to 5; Fig. 7 and Table 3 in Appendix 1) with a wide range of grainsize distributions, but always characterized by the presence of a mud fraction (silt + clay) largely > 20 wt%. The poor sorting nature does not change with distance (Figs. 6a, b, 7). Pyrite grains in matrix are observable in hand specimens. Yellow-colored patches, probably of native sulfur and/or precipitation from pore water in relation to dissolved sulfide and sulfate minerals, are also observed. The deposits contain granules to cobbles; however, 30-cm-sized to 1-m-sized boulders are also included. Clasts are mainly composed of unaltered andesite with subordinate amounts of white-colored hydrothermally altered rocks of angular shape up to 3 cm in diameter. Juvenile materials such as pumice, scoria, and fresh glass shards are not recognized. Usually, sediments are porous and < 1 mm spherical voids are present (Fig. 4f) that suggest air bubble vesicles within debris flow deposits (Fisher and Schmincke 1984, page 306; Harpel et al. 2013). Standing trees, wood logs, and shrubs that had been part of the riparian forests at the time of eruption were incorporated with the lahar deposits.

Poor sorting, massive facies, and trapped air in the matrix of the October lahar deposits, as well as very high clay content within sand + silt + clay fraction of the deposits (10–20%: Fig. 7d, Table 3 in Appendix 1),

(See figure on next page.)

Fig. 4 Field photographs showing the occurrence of the October lahar (muddy, cohesive debris flow: MF) deposits. **a** Overbank deposits in the Nigorigawa River. The photograph was taken on November 12, 2014, when the river was turbid. **b** Wrinkles over the surface of the lahar deposits at Loc. 1194. **c** Lahar deposits (MF) of in-channel facies directly overlie the pre-eruptive (p.e.) fluvial gravel (openwork, clast supported) at Loc. S119. Photograph (May 30, 2015) showing turbidity of the river. **d** Lahar deposits (MF) of in-channel facies at Loc. S114. **e** Close-up of the lahar deposits showing massive and muddy matrix supported nature, Loc. S119. **f** Air bubble vesicles in the muddy matrix, Loc. 1192. **g** Fringe of the lahar deposits (overbank facies), Loc. 1004. **h** Close-up of the lahar deposits of overbank facies, Loc. 1004. **h** Distal end of the lahar deposits, Loc. 1207

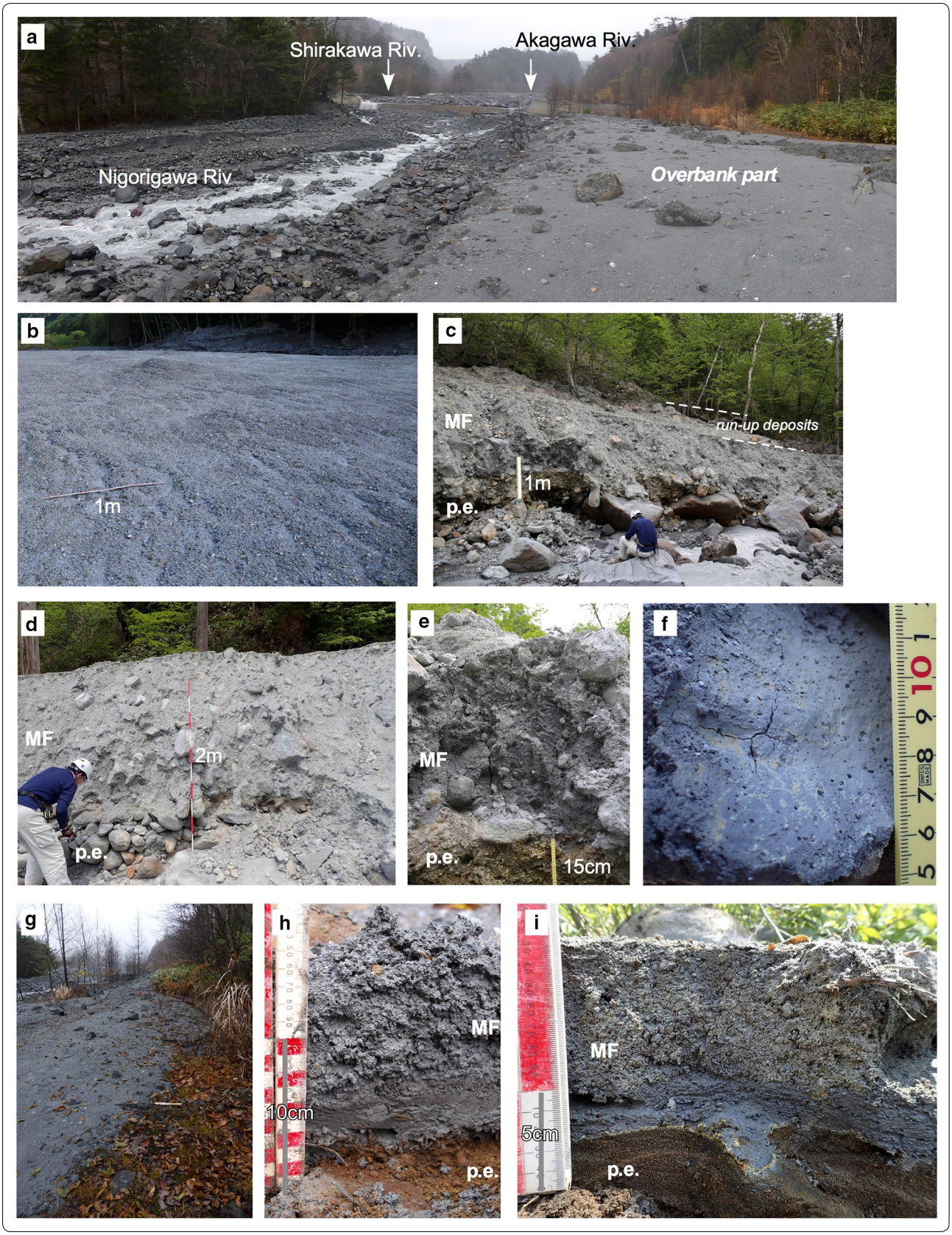
a
Shirakawa Riv.
Akagawa Riv.
Nigorigawa Riv
Overbank part
b
1m
c
MF
run-up deposits
1m
p.e.
d
MF
2m
p.e.
e
MF
p.e.
15cm
f
g
h
MF
10cm
p.e.
i
MF
5cm
p.e.

indicate a cohesive debris flow (Scott et al. 1995; Vallance and Scott 1997; Vallance and Iverson 2015). The clay content slightly decreases toward downstream (Fig. 7d). No major facies changes in vertical sections and proximal to distal sections (Fig. 6a, b) indicate the absence of flow transformation into hyperconcentrated flow and/or sediment-laden streamflow during flow. The absence of flow transformation is more common in cohesive debris flows than cohesionless debris flows (Scott et al. 1995; Vallance and Scott 1997; Sohn et al. 1999).

Mineral and chemical characteristics

Matrix sediments of 1/4–1/8 mm fraction consist mainly of white hydrothermally altered lithic fragments sometimes attached to smaller pyrite aggregates, and feldspars. Brown-colored lithic fragments, quartz, and pyrite are present. Trace amounts of orthopyroxene and clinopyroxene are recognized.

Bulk chemistry indicates that the October lahar deposits contain 10–14 wt% sulfur (Fig. 8, Table 4 in Appendix 2), which is conspicuously higher than that of pre-eruption fluvial deposits (0.3–4.1 wt%). Mineral assemblages identified by XRD comprise quartz, plagioclase, cristobalite, pyrite, gypsum, anhydrite, alunite, pyrophyllite, smectite, illite, kaolin group minerals (7Å), illite/smectite mixed layer, and chlorite (Table 2). Some of these are typical of eruption material derived from hydrothermally altered areas in Japanese volcanoes (Ohba and Kitade 2005). The composition of the lahar samples is similar to that of primary ashfall deposits of the 2014 eruption at Ontake (Table 2; Minami et al. 2016) and indicates that lahar deposits contain primary eruption (ashfall and pyroclastic density current) deposits derived from hydrothermally altered materials on surface and/or beneath the vents.

Description of the rain-on-snow-triggered lahar and deposits on April 20, 2015

Overview

According to the public announcement by the Forestry Agency (http://www.rinya.maff.go.jp/chubu/press/kouhou/150420_2.html), the debris flow alert system was again activated by a flow at 8:08 p.m. on April 20, 2015. The wire sensor at the time was set at almost the same place to the previous site (Fig. 1), but at slightly higher position at 1.4–2.0 m above the riverbed than when the October 2014 lahar was detected.

At the Tanohara rain gauge (at 2190 m. a.s.l.), 278 mm of heavy rain was observed from 7:00 a.m. on April 20 to 3:00 a.m. on April 21 (Fig. 2b). The warm, humid, and windy weather condition was due to an extratropical cyclone. It caused rainstorm and snow melting, and hence, the snowpack around the weather station completely disappeared by the end of the rainstorm (Fig. 2a, b). The ROS event caused the snowmelt of 120 mm water equivalent, and thus, the total water input (rainwater + meltwater) was 398 mm. Cumulative rain + meltwater until lahar initiation (~ 8 p.m.) was 234 + 98 mm over 13 h, and peak input of 35 mm/h occurred during the period from 2 p.m. to 6 p.m. Snow depth at Tanohara became less than 10 cm after 6 p.m. The rate of water input was sufficient to trigger a lahar. The increase in flow discharge in the Akagawa River was observed by the time-lapse camera records (Fig. 1: nearby Loc. 1227, and supplementary movie as Additional file 1) although the peak flow at night could not be recorded.

Deposits

Bank erosion by the ROS-triggered lahar was mainly in the upstream part of the Akagawa River (Fig. 9a). The preexisting depositional sequences emplaced by the October muddy lahar deposits and pre-eruptive terrace deposits were highly eroded and exhumed by the ROS lahar flow (Figs. 5b, 9a, b). Locally original riverbed was filled with sand and gravel causing > 1 m aggradation. At Loc. 1227, where the time-lapse camera was installed, the lahar flow partly eroded the October lahar terrace and left new lahar deposits with 50 cm thickness (Figs. 5a, 9c, d). The authors' regular ground survey confirms that there was no relevant deposit on April 15, 2015, but the presence of the ROS lahar deposits was confirmed on May 19 (Fig. 9c, d). The camera records and meteorological observations at Tanohara provide evidences that there were no ROS major flood events after April 20 to May 19. Therefore, the sedimentary sequence observed on May 19 displays the ROS-triggered lahar deposits.

The ROS lahar deposits show crude horizontal stratifications and/or low-angle cross-stratifications (Figs. 6a, b, 9d, e) at Loc. 1227 (~ 5 km from vents) and Loc. 1228–1229 (7 km). The sedimentary facies is indicative of hyperconcentrated flow deposits (Smith 1986; Pierson 2005). The deposits mainly consist of very coarse sand to granules with medium sand and fine pebbles. They are moderately to poorly sorted ($\sigma_I = 0.9$ to 2.6) and depleted in mud (Figs. 6a, b, 7, and Table 3 in Appendix 1). Clasts in lahar deposits are mainly of andesite. They are mostly round, and some clasts have

(See figure on next page.)

Fig. 5 Schematic sections showing the stratigraphy of the October 2014 rain-triggered and April 2015 ROS-triggered lahar deposits. **a** At Loc. 1227 in the Akagawa River, **b** after confluence of the Shirakawa and Akagawa Rivers, and **c** at the distal end of the Nigorigawa River

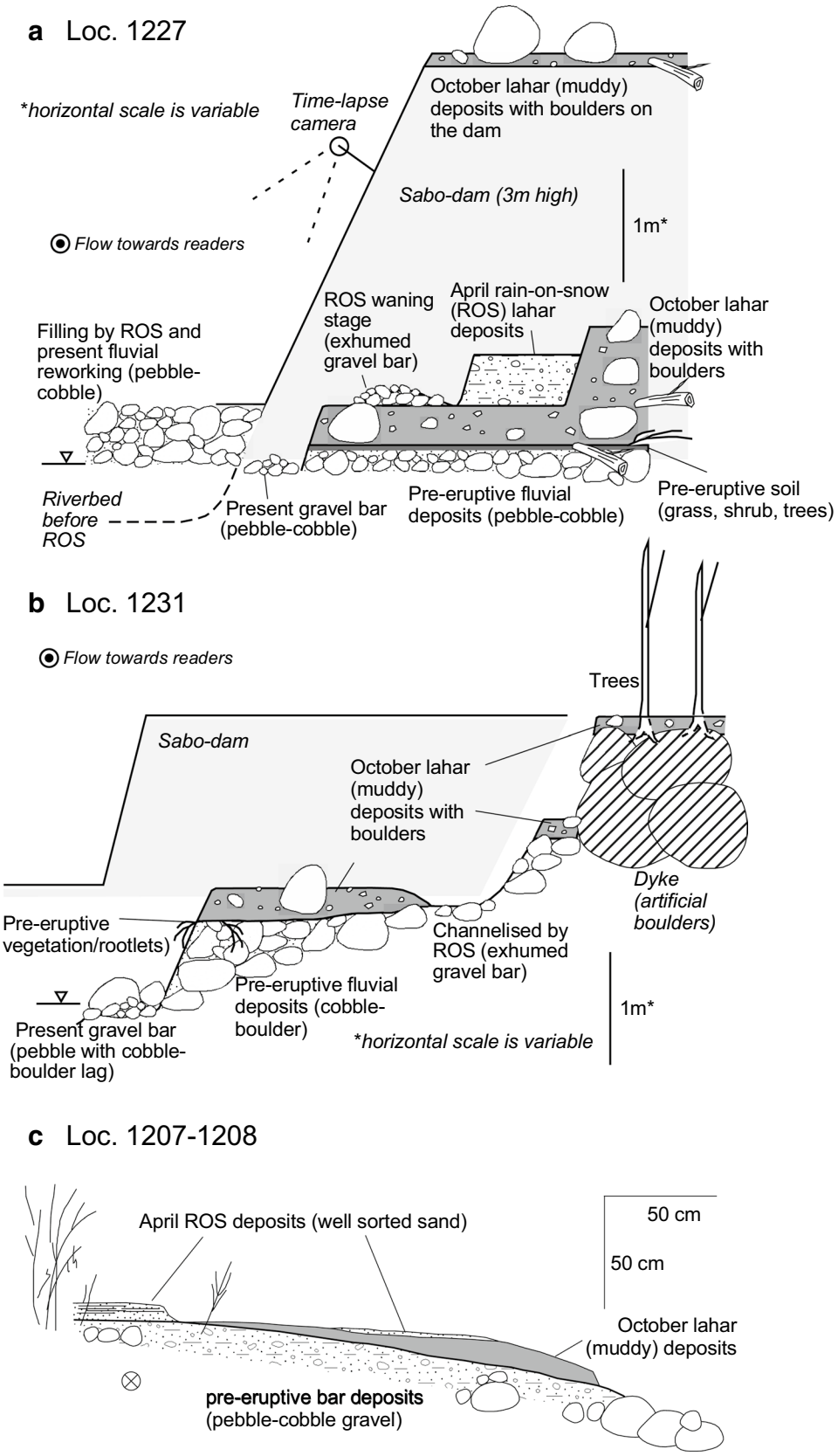
a Loc. 1227
*horizontal scale is variable
Time-lapse camera
October lahar (muddy) deposits with boulders on the dam
Sabo-dam (3m high)
1m*
Flow towards readers
ROS waning stage (exhumed gravel bar)
April rain-on-snow (ROS) lahar deposits
October lahar (muddy) deposits with boulders
Filling by ROS and present fluvial reworking (pebble-cobble)
Riverbed before ROS
Present gravel bar (pebble-cobble)
Pre-eruptive fluvial deposits (pebble-cobble)
Pre-eruptive soil (grass, shrub, trees)
b Loc. 1231
Flow towards readers
Trees
Sabo-dam
October lahar (muddy) deposits with boulders
Dyke (artificial boulders)
Pre-eruptive vegetation/rootlets)
Channelised by ROS (exhumed gravel bar)
Pre-eruptive fluvial deposits (cobble-boulder)
1m*
Present gravel bar (pebble with cobble-boulder lag)
*horizontal scale is variable
c Loc. 1207-1208
April ROS deposits (well sorted sand)
50 cm
50 cm
October lahar (muddy) deposits
pre-eruptive bar deposits
(pebble-cobble gravel)

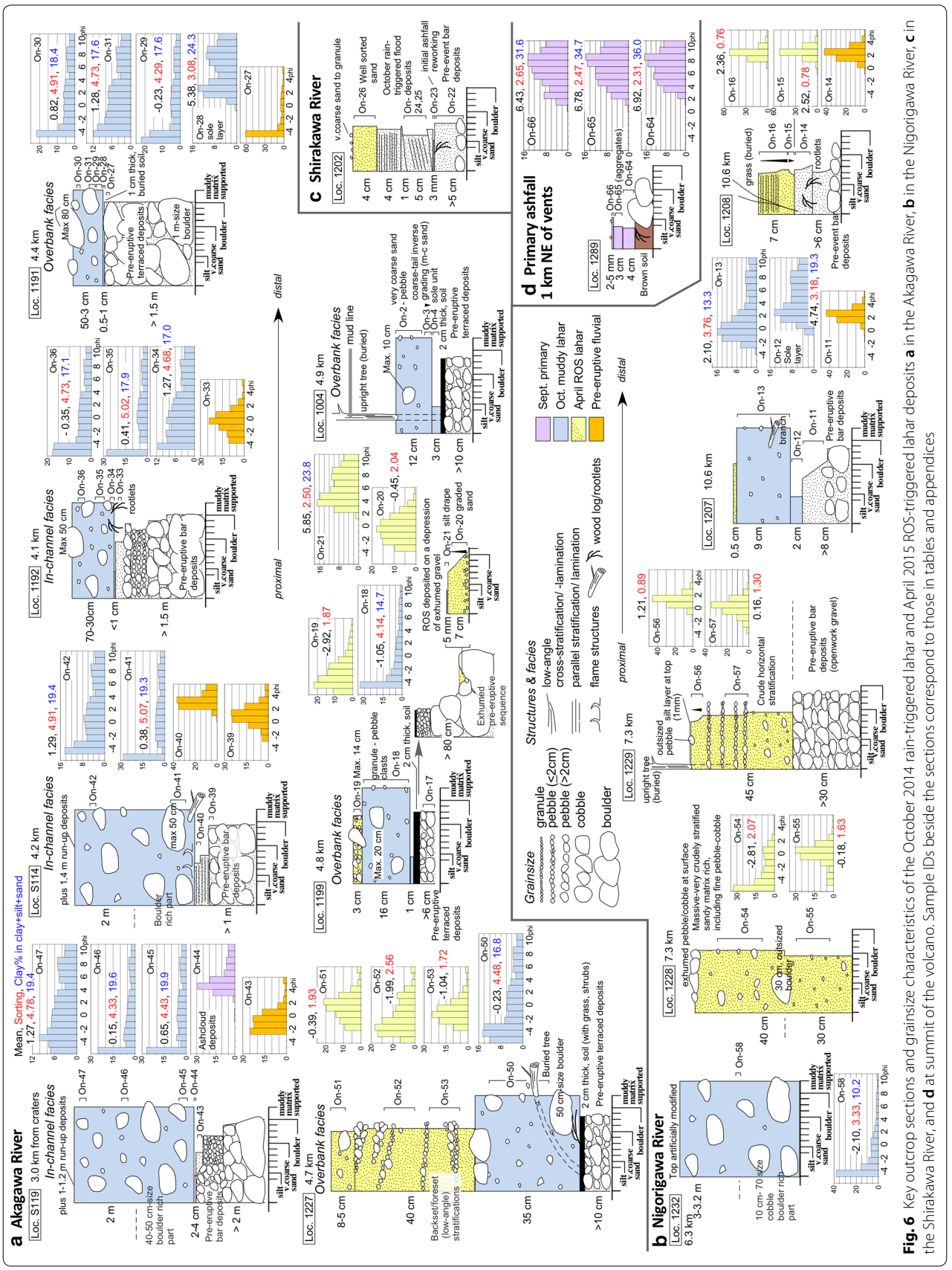

Fig. 6 Key outcrop sections and grainsize characteristics of the October 2014 rain-triggered lahar and April 2015 ROS-triggered lahar deposits **a** in the Akagawa River, **b** in the Nigorigawa River, **c** in the Shirakawa River, and **d** at summit of the volcano. Sample IDs beside the sections correspond to those in tables and appendices

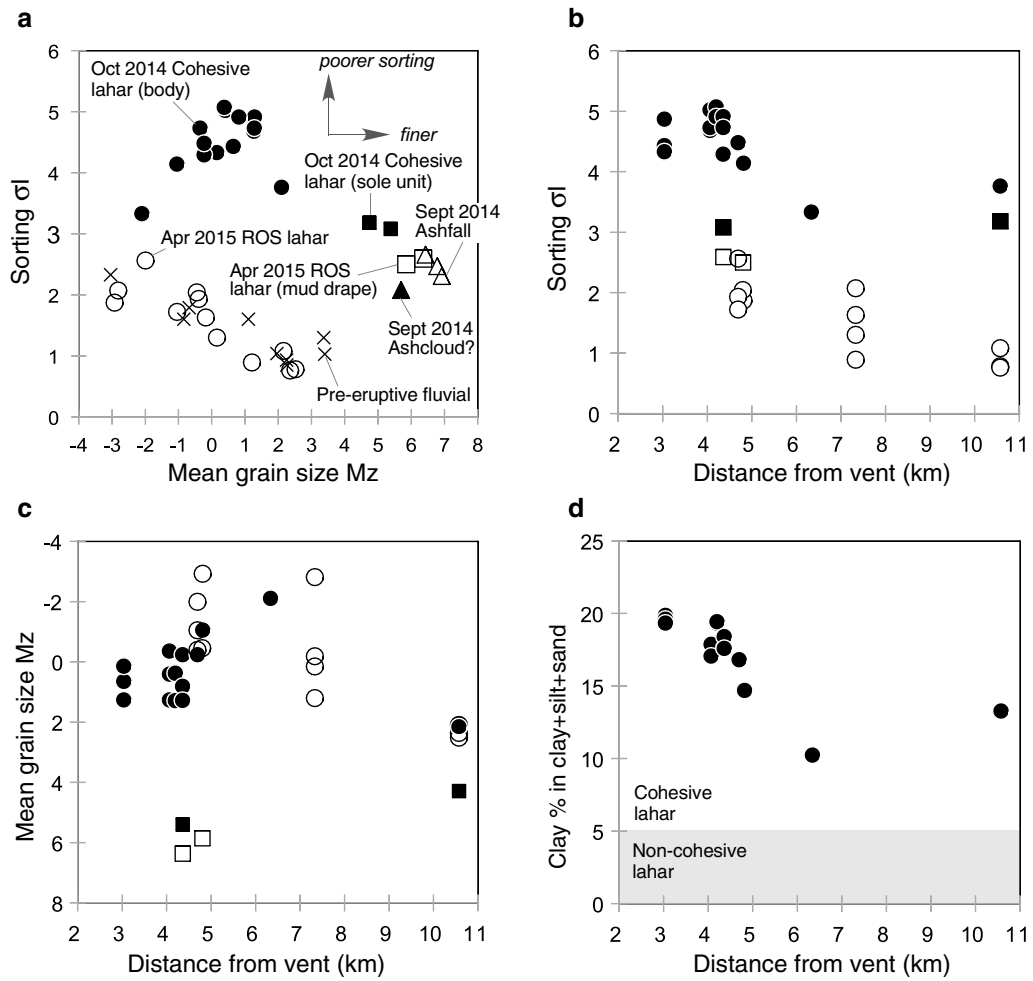

Fig. 7 Grainsize characteristics of pre-eruptive, 2014 eruptive and post-eruptive lahar deposits in the Akagawa and Nigorigawa Rivers and around Ontake Volcano. **a** Sorting and mean grainsize of samples. **b** Sorting and **c** mean grainsize versus distance from the Jigokudani vents for samples of October 2014 rain-triggered and April 2015 ROS-triggered lahar deposits. Note that the samples from debris flow deposits represent grainsize less than cobble because of limitation of sampling of larger clasts at the field. **d** Percentage of clay in clay + silt + sand fractions in the October lahar deposits

weathering (oxidized) rind indicative of entrainment of exposed river gravel and/or terrace deposits during flow travelling. Angular fine pebbles to granules, in white color, of hydrothermally altered rock origin, are also present. At the Loc. 1199, the ROS lahar deposits, directly overlying the October lahar deposits, are 3–7 cm thick (Fig. 9f). Gray mud drapes, less than 1 cm thick, are locally observed on the top of the sandy ROS lahar deposits (Fig. 6a, Loc. 1199).

The distal lahar deposits (10.5 km from the vents), 2–7 cm thick, consist of relatively better-sorted sand with parallel lamination ($\sigma_I = 0.8$: Table 3 in Appendix 1, Figs. 6b, 7a, b, 9g), indicative of upper flow regime sedimentation under a normal streamflow condition (Allen 1982; Smith and Lowe 1991). The deposits directly overlie the October lahar and pre-eruptive fluvial bar deposits (Figs. 5c, 6b). Sorting values (σ_I) and mean grainsize of the lahar deposits decrease with distance (Fig. 7b, c).

The thickness of the ROS lahar deposits is clearly less than that of the October lahar deposits. Therefore, the total volume for the deposits is smaller than that of the October lahar. On the other hand, the total discharge (water input + sediment) of the ROS lahar must be larger because of the highly erosive nature of the flow and extremely large water input in the catchment.

Mineral and chemical characteristics

Matrix sediments of 1/4–1/8 mm fraction comprise gray, brown, white angular to sub-angular lithic fragments and fresh angular feldspar grains. Pyrite grains as well as white hydrothermally altered lithic fragments attached to smaller pyrite aggregates are found, but are

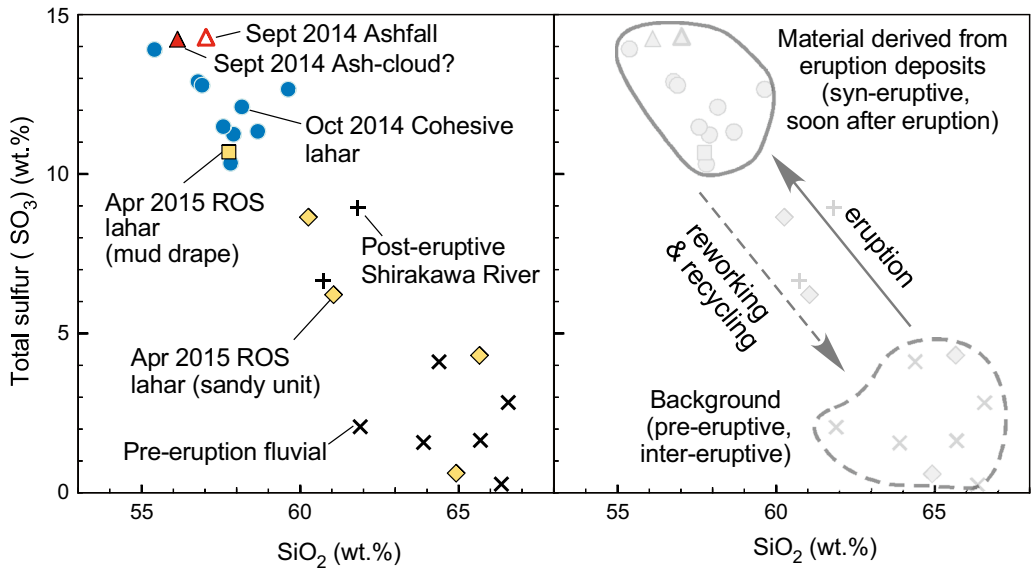

Fig. 8 Plot showing total sulfur content (as SO_3) versus SiO_2 content in ashfall, October rain-triggered and April ROS-triggered lahars, and pre-eruptive fluvial deposits

Table 2 Mineral assemblages of 2014 primary eruption, October rain-triggered lahar, and April ROS-triggered lahar deposits identified by XRD

Sample name	Description	Qz	Pl	Crs	Py	Gp	Anh	Alu	Prl	Sme	Ilt	Kln	I/S	Chl
September 2014 primary deposits														
On-1	Ashfall (Tanohara parking lot; bulk)	+	+	+	+	+	+	+		+	+	+		
On-64	Ashfall (Ishimuro Sanso hut; lower part)	+	+	+	+	+	+	+	+	+		+		
On-65	Aggregates of ashfall (Ishimuro Sanso hut; upper part)	+	+	+	+	+	+	+	+		+	+		
On-44	Ash cloud deposits (Akagawa, upstream end)	+	+	+	+	+	+	+	+	+	+	+		+
October 2014 rain-*triggered lahar*														
On-13	Cohesive debris flow deposits (Nigorigawa, downstream end)	+	+	+	+	+	+	+	+	+	+	+	+	+
On-18	Cohesive debris flow deposits (Akagawa, overbank facies)	+	+	+	+	+	+	+	+	+		+	+	+
On-34	Cohesive debris flow deposits (Akagawa, bottom part)	+	+	+	+	+	+	+	+	+	+	+		+
On-45	Cohesive debris flow deposits (Akagawa, upstream end)	+	+	+	+	+	+	+	+	+	+	+	+	+
April 2015 rain-on-snow-triggered lahar deposits (mud drape)														
On-21	Rain-on-snow lahar deposits (Akagawa)	+	+	+	+		+	+	+	+	+	+	+	+

Qz quartz, *Pl* plagioclase, *Crs* cristobalite, *Py* pyrite, *Gp* gypsum, *Anh* anhydrite, *Alu* alunite, *Prl* pyrophyllite, *Sme* smectite, *Ilt* illite, *Kln* kaolin group minerals (7Å), *I/S* illite/smectite mixed layer, *Chl* chlorite

less prominent than those in the October lahar deposits. Locally well-rounded semitransparent mineral grains (weathered feldspars) are present. Trace amounts of orthopyroxene and clinopyroxene grains are recognized.

The total sulfur content in the ROS deposits varies from 0.6 to 8.7 wt%. The value is intermediate between those of pre-eruptive fluvial deposits (<4.1 wt%) and October lahar deposits (>10 wt%: Fig. 8 and Table 4 in

(See figure on next page.)

Fig. 9 Field photographs of the April ROS-triggered lahar deposits. MF: October lahar deposits, p.e.: pre-eruptive fluvial deposits, and ROS: April lahar deposits. **a** Retreated bank (arrow) showing high erosional character of the lahar flow. **b** Exhumed pre-eruptive terrace deposits and the October lahar deposits. **c** The ROS lahar terrace (Loc. 1227) developed into the October lahar deposits overlying the pre-eruptive fluvial deposits. **d** Close-up of **c**. **e** Massive to very crudely stratified ROS deposits indicative of hyperconcentrated flow deposition (Loc. 1229). **f** Thin ROS lahar deposits (overbank facies) overlying the October lahar deposits (Loc. 1199). **g** Distal end of the ROS deposits. The deposits are well sorted and parallel laminated (Loc. 1208)

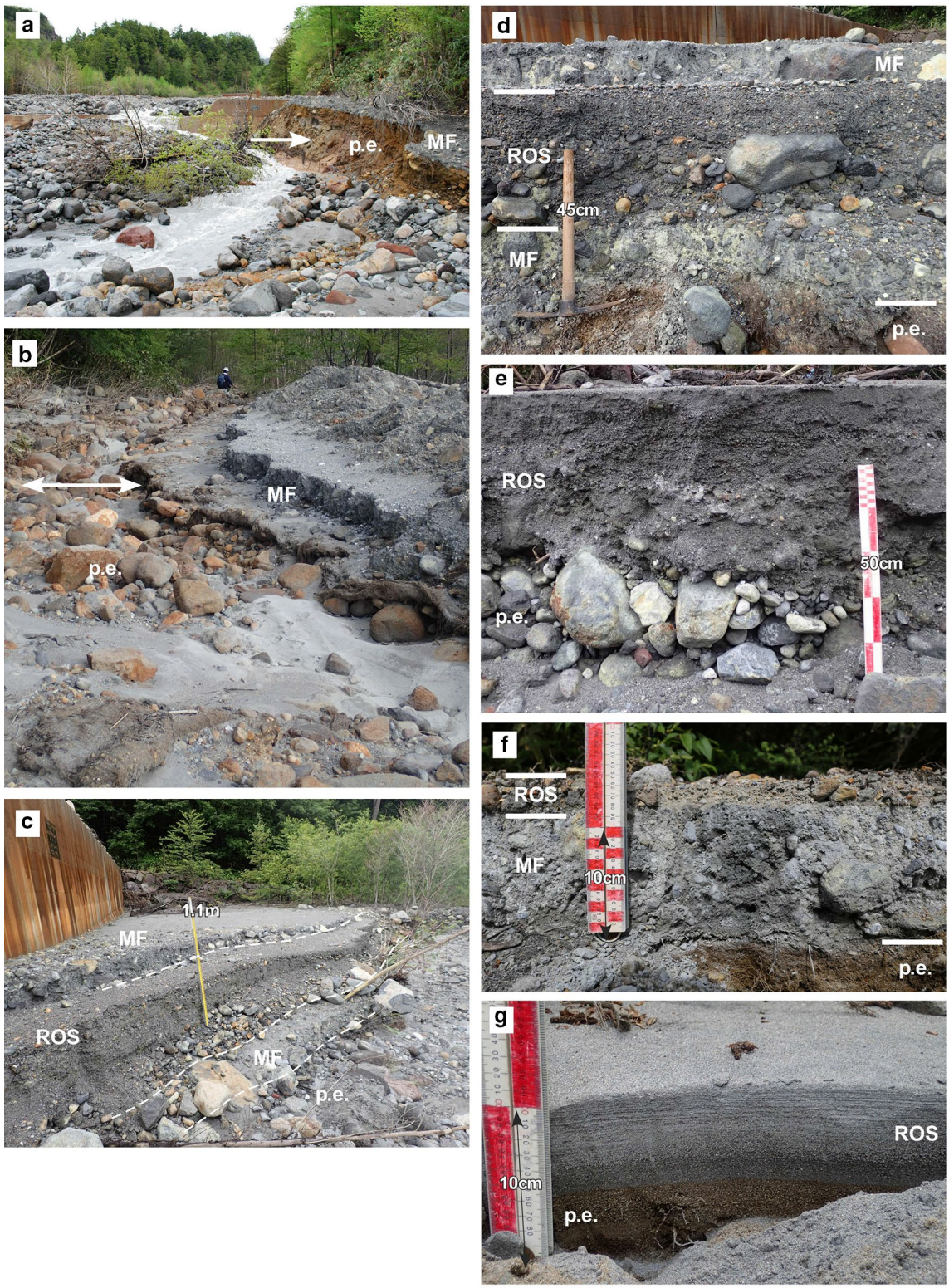
a
p.e.
MF
b
MF
p.e.
c
1.1m
MF
ROS
MF
p.e.
d
MF
ROS
45cm
MF
p.e.
e
ROS
50cm
p.e.
f
ROS
MF
10cm
p.e.
g
ROS
10cm
p.e.

Appendix 2). The only exception is found from the mud drape part, which contains 10.7 wt% of sulfur. Mineral assemblages for the mud drapes of ROS deposits examined by XRD show similarity with those in the October lahar deposits, such as quartz, plagioclase, cristobalite, pyrite, anhydrite, alunite, pyrophyllite, smectite, illite, kaolin group minerals (7Å), illite/smectite mixed layer, and chlorite (Table 2).

Sediments in the Shirakawa River and pre-eruptive fluvial deposits

No typical cohesive debris flow deposits by the October lahar could be observed during the ground survey in the upper reach of the Shirakawa River. There was a post-eruptive deposit consisting of three units in ascending order (Fig. 6c: Loc. 1202): (1) blue-gray- to gray-colored muddy deposit with less than 1 cm thickness derived from initial ashfall reworking at the bottom; (2) a 10-cm-thick, parallel to cross-laminated sandy unit of probable flood deposits on October 5; and (3) washed (well-sorted) 4-cm-thick sand unit, of ROS-related small-runoff origin, occupying the topmost sequence.

Pre-eruptive fluvial (some terraced) deposits in the Akagawa, Shirakawa, and Nigorigawa Rivers are described and analyzed similarly in order to compare with lahar event deposits (Fig. 6a–c and Table 3 in Appendix 1). They basically comprise well-rounded to sub-rounded andesite clasts (pebble to boulder) with sand matrix as parts of gravel and sand bars within channels. Bulk chemistry shows low sulfur content (0.3–4.1 wt%: Fig. 8 and Table 4 in Appendix 2). Sandy matrix sediments in 1/4–1/8 mm fraction comprise mainly reddish brown to brown color lithic fragments with subordinate amounts of feldspar and trace amounts of orthopyroxene and clinopyroxene.

Interpretations for lahar events on and after the 2014 eruption: triggers, flow and depositional characteristics, and origin of sediments

Syn-eruptive lahar on September 27, 2014

The air-borne survey (Sasaki et al. 2016) indicates a syn-eruptive lahar, which occurred adjacent to the Jigokudani vents and travelled about 5 km downstream. The lahar trigger was initiated by (1) expelled mud slurries from vents combining to form a lahar (Sasaki et al. 2016) and/or by (2) a pyroclastic density current travelling down to the head of the Akagawa River and transforming into a lahar. Despite the possibility of the lahar derived from a pyroclastic density current, Sasaki et al. (2016) concluded that relatively long runout of the muddy lahar required it to originate directly from the vents. The detailed description of two post-eruptive lahar deposits by the present study reveals that the impact of the syn-eruptive lahar was limited and smaller than that discussed in Sasaki et al. (2016). Their ground survey was carried out for 10 months (i.e., long after the April ROS-triggered lahar event) after the eruption. They observed and took samples of what they considered as the syn-eruptive lahar deposits from Sites A, B, C, and D (Sasaki et al. 2016). These localities, which are situated near to Loc. 1192, S114, 1227, and 1232-2 in the present study, respectively, were already impacted by the October and April lahars. The Site D is even outside of the distribution of the syn-eruptive lahar according to the air-borne survey. The 1.2×10^5 m^3 volume proposed for the syn-eruptive lahar deposits is overestimated by the representative deposit thickness of 1 m (Sasaki et al. 2016), because the thickness represents that of the October lahar deposits. The syn-eruptive mud slurry had to be very thin, on the basis of oblique aerial photographs taken immediately after the eruption (Figure 3e in Sasaki et al. 2016). A field photograph (Figure 5b in Sasaki et al. 2016) taken during ground survey by the Forestry Agency on October 2, 2014, just before the October 5 lahar confirmed thickness of the syn-eruptive deposits to be less than 10–15 cm, and volume is reassessed as $< 1.2–1.5 \times 10^4$ m^3. Other photographs (Figure 5a, d–h in Sasaki et al. 2016) taken during the survey of 10 months after the eruption show only top surfaces of the deposits, i.e., the overbank facies of the October lahar deposits. This means that these photographs do not indicate the syn-eruptive lahar deposits, which should be appeared in the lower part of the depositional sequences. Thus, they described the October rain-triggered lahar and its deposits as the syn-eruptive ones. Most of the syn-eruptive mud slurry deposits were probably buried and/or degraded by post-eruptive lahars and fluvial reworking. The possible implication for the presence of the syn-eruptive lahar is thin and fine-grained deposits described here as a sole layer and/or ash cloud deposits underlying the main body of the October lahar deposits in the upstream area of the Akagawa River (Loc. S119, 1192, and 1191). However, distinguishing these deposits from the October lahar deposits is difficult due to the lack of direct observation immediately after the syn-eruptive lahar.

The October rain-triggered lahar deposits described in Sasaki et al. (2016) are gravelly and not muddy indicative of the April ROS lahar or fluvial deposits (Figure 5f in Sasaki et al. 2016). This also indicates that part of facies and compositional descriptions (petrography and mineral assemblages) as well as grainsize data of the lahars and their deposits described in Sasaki et al. (2016) needs to be reconsidered and carefully cited. Rather than the syn-eruptive lahar, other two post-eruptive lahar events described in the present study were more significant to

the river system and hazardous in terms of long runout and volume of deposits.

Rain-triggered lahar on October 5, 2014

The October 2014 lahar was triggered not by the first rainstorm, but by the second rainstorm associated with a typhoon on October 5 when for the first time > 10 mm/h precipitation was recorded after the eruption. The delayed response is probably due to the characteristics of ashfall of the 2014 eruption. Very high clay content (32–36 wt%) and the presence of clay minerals in the September ashfall deposits (Fig. 6d and Table 2 and Table 3 in Appendix 1) are due to hydrothermal alteration of source material. The clay-rich nature resulted in resistance to erosion of the cohesion ash surface (Wischmeier and Smith 1978; Goldman et al. 1986) by the first rainstorm event, with peak intensity of 6.9 mm/h and total 52.5 mm precipitation. The physical properties of eruption deposits constrain permeability and erodibility of surface exposures (Pierson and Major 2014). Nomura et al. (2003) discussed that a similar cohesive ash-covered landscape suppressed lahar initiation after the 2000 phreatomagmatic eruption at Mt. Usu. In contrast, the 2008–2009 magmatic eruption at Chaitén volcano produced granular primary tephra which was cohesionless and susceptible to erosion. The ashfall over hillslopes was easily eroded with small precipitation (20 mm per day), causing a lahar and acute sedimentary response to rainfall events (Pierson et al. 2013).

Due to the October 5 rain and lahar event, most of the primary sediments in upslope area were swept away (Fig. 3a, b), which could lessen the opportunity to generate other rain-triggered lahars in the same rainy season. Indeed, other heavier rainfall and ROS events with cumulative rainfall + snowmelt > 100 mm after the October lahar event could not trigger any significant lahars in the river system until the last ROS event on April 20, 2015, with rainfall and snowmelt totaling 332 mm immediately prior lahar (Fig. 2).

Despite the similarity of geomorphological and hydrological features of the Shirakawa River and Akagawa River as well as the ashfall deposition that was also observed in the Shirakawa River headwaters, there were no lahar deposits along the Shirakawa. In contrast to the Shirakawa River, the head of the Akagawa catchment hosts the active volcanic vents, suggesting that deposition of pyroclastic density current deposits and 10s-cm-thick proximal pyroclastic fall deposits was critical for lahar generation in the Akagawa River. The isopach map for the pyroclastic fall deposits by the September 2014 eruption (Fig. 1a) also suggests that headwater catchment of the Akagawa received 2×10^5 m^3 of ashfall, whereas ashfall deposited in the Shirakawa headwater is only 2×10^3 m^3. Thus, the Shirakawa River catchment was less impacted by the eruption.

Visible amounts of pyrite and native and/or precipitated sulfur in the October lahar deposits, along with the extremely high sulfur contents and diagnostic clay mineralogy, indicate that the lahar deposits were derived from remobilized 2014 eruption deposits, which included hydrothermally altered materials. Clay minerals such as smectite and kaolin group minerals and the unusually high clay content in deposits definitely contributed to the viscosity of the flow (Hampton 1975; Pierson 2005). Even after selectively depositing large clasts at the confluence of the Denjogawa River, the fine part (i.e., matrix part) of cohesive October lahar was able to travel longer distance without flow transformation because high viscosity can damp turbulence (Baas et al. 2009, 2011) and hamper dilution of the lahar with river water (Fig. 10).

Rain-on-snow-triggered lahar on April 20, 2015

The ROS-induced lahar on April 20 was the largest flow event during the snowmelt season in 2015 in the Akagawa and Nigorigawa Rivers. The conditions were most conducive for generating a lahar. Contributing factors include (1) the very high rate of water delivery to the catchment (rain plus snowmelt), (2) the availability of a supply of older loose sediments, in addition to those remaining after the 2014 ashfall and lahar, and (3) new exposures of these available sediments following removal of snow cover at almost the end of the snowmelt season.

The ROS-triggered lahar on April 20 was caused by the largest rainstorm during the 24 months after the eruption (Fig. 2c), resulting in the total water input (rain + snowmelt) of 398 mm. The warm, moist, windy conditions during ROS events produced substantially higher energy for snow melting which came from sensible and latent heat exchanges (e.g., Marks et al. 1998, 2001). Debris flows and significant floods triggered by the augmentation of water input to a hydrological system under the ROS situation have been previously reported in other volcanic and non-volcanic regions (e.g., Marks et al. 2001; Sobieszczyk et al. 2008).

In contrast to the October lahar, the ROS-triggered lahar was dilute due to (1) large total water input resulting in high discharge of the flow, (2) the shortage of slope-covering and valley-confined primary eruptive deposits, most of which already was removed by the October lahar event, and (3) the paucity of clay in the flow. The dilute lahar was erosive during travelling so that it was able to incorporate the October lahar deposits in the valley as well as gravelly river and terrace deposits (Fig. 10). This is supported by the sedimentary composition of the ROS lahar deposits which

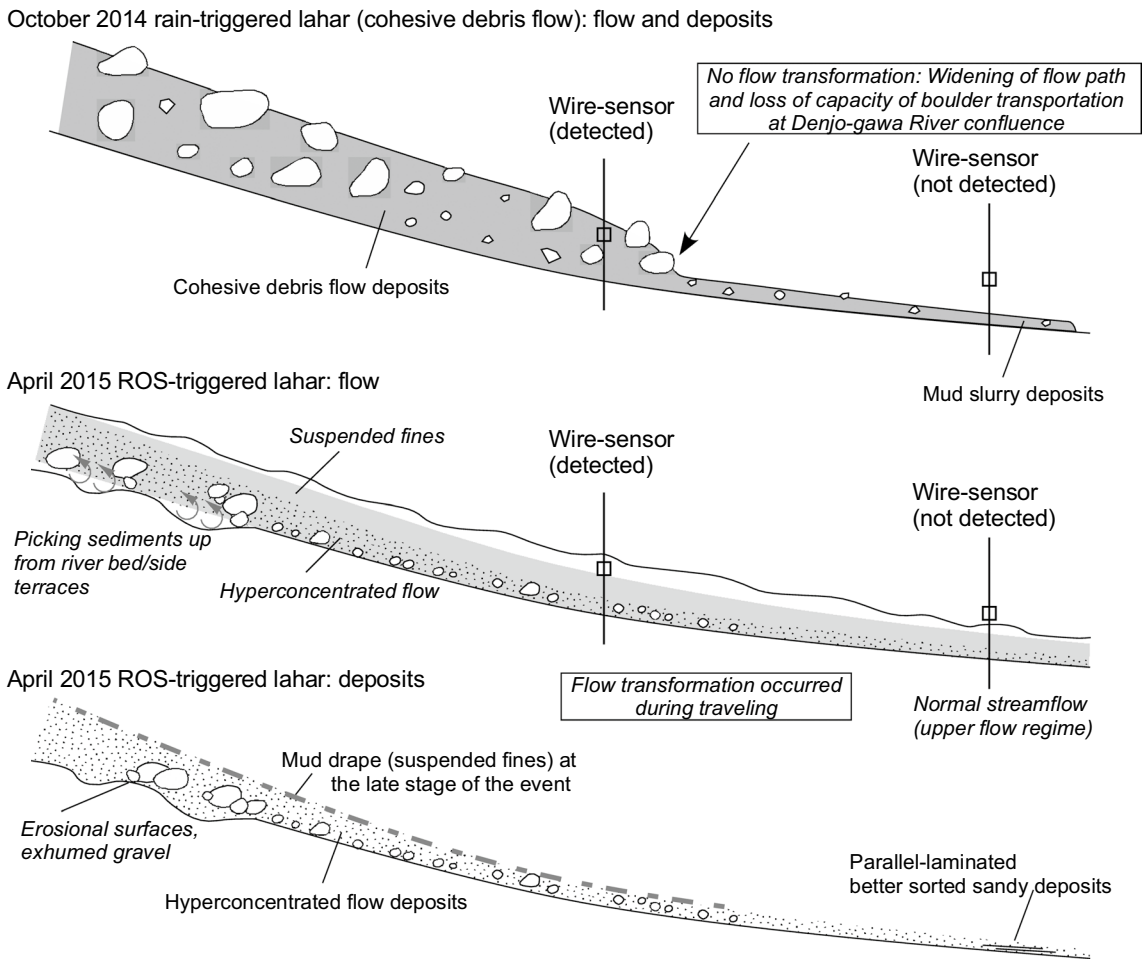

Fig. 10 Schematic illustration showing flow and depositional characteristics of two post-eruptive lahars in the Akagawa and Nigorigawa Rivers

consist of fines-poor sand and gravel, rich in rounded pebbles and cobbles originating from preexisted fluvial deposits, as well as sediments derived from the October lahar deposits. The initial flow could not entrain enough sediment to turn into debris flow. It evolved instead into hyperconcentrated flow, which finally (by deposition along its flow path) transformed into normal streamflow at the distal locality (Fig. 10). The ROS conditions causing cohesionless debris flows and/or hyperconcentrated flows in volcanic regions have been documented previously (Pringle and Scott 2001; Sobieszczyk et al. 2008). Mud drapes on the sandy or gravelly ROS deposits indicate condensed suspension fines, which is typical of hyperconcentrated flows (Pierson 2005).

Thickness of snowpack over sediments/rock was also a significant factor to generate a ROS-triggered lahar. There were other two ROS runoff events (on March 19 and April 3) resulting in stage changes in the rivers in the snow season (Fig. 2a). However, these two events did not generate a lahar. Although the ROS situation on March 19 and April 3 enhanced snowmelt too, there was still a > 1-m-thick snowpack on upper slopes after the ROS events (Fig. 2a), suggesting most of the available sediments were still covered with snow. In contrast, only a 10-cm-thick snowpack was recorded 2 h before the ROS-triggered lahar generation on April 20 (Fig. 2b). These indicate that sediments were newly exposed after the removal of snow cover, and consequently, combined with other factors, the condition was favorable to generate a lahar in the end of the snowmelt season.

Discussion

Factors and timing of lahars after an eruption at a seasonally snow-clad volcano

At permanently snow-clad volcanoes, eruption-triggered lahars with snow and glacier melting can pose serious lahar hazards, for example, the 1985 eruption of Nevado del Ruiz (Pierson et al. 1990). However, a snow-clad

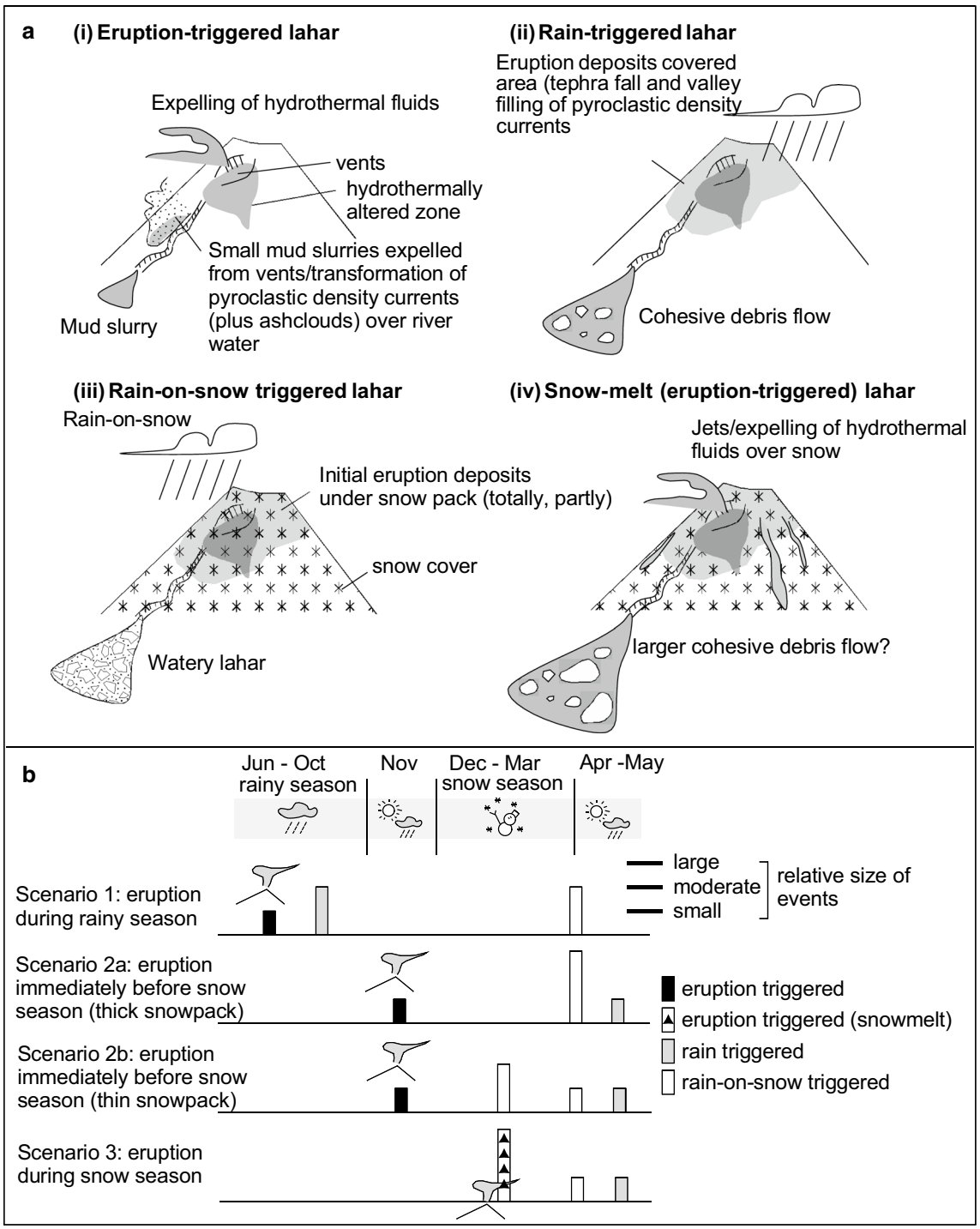

Fig. 11 Schematic models showing **a** observed (i to iii) and possible (iv) lahar events for syn-eruptive and post-eruptive periods at Ontake Volcano and **b** observed Scenario 1 and predicted Scenarios 2a, 2b and 3 of lahar events of the volcano when a similar scale of 2014 phreatic eruption recurs

volcano with "seasonal snow/ice" such as Ontake Volcano has complex lahar-triggering and driving factors such as rainfall, snowfall, and snowmelt which vary in the seasons (Fig. 11a).

The Ontake 2014 eruption aftermath clearly shows that the timing of eruption (i.e., whether it occurs in the rainy season, snow season, or snowmelt season) can affect flow types and size of lahars (Fig. 11a(i), (ii), (iii), and Scenario

1 of Fig. 11b) and suggests the predicted scenarios for lahars (Scenarios 2 and 3). Although at Ontake Volcano, post-eruptive lahars may occur during the rainy season, a ROS condition especially at the end of snowmelt season should be much more hazardous because of the compounding effect of rainfall and meltwater, whereas during the snow season, the availability of sediments, to be picked up and transported by surface water runoff, decreases because of thick snow accumulation over the deposits. It is assumed that if the 2014 eruption had happened at the end of the rainy season and before the snow season (Scenario 2a), then primary eruption deposits on slopes as well as pyroclastic density current deposits confined in the valley would have been stored under the snowpack. Eventually, a ROS-induced lahar could have been larger than the October rain-triggered lahar and the April ROS-triggered lahar, with an end-of-season sudden release of eruption deposits stored on upslope areas. The snow season in 2014/2015 was characterized by conspicuously thick accumulation of snow in contrast to the next year (2015/2016) which had less snow (Fig. 2c). If there were lesser snow accumulation after the eruption of Ontake, rain could occasionally have occurred instead of snow during the snow season, which could result in several small ROS-induced lahars (Scenario 2b). The ROS situation is common at Ontake and was not unique during the year 2014/2015 (Fig. 2c); however, there are no reports of other ROS-induced flood and debris flows and their deposits, which influenced the Nigorigawa River catchment. This denotes that the potential of (1) the initiation of a ROS-induced flow event and (2) preservation of ROS-related deposits can be higher only when an explosive eruption "adds" excess eruptive and sedimentary materials on surfaces. Syn-eruptive lahars associated with snow-melting water at Ontake Volcano have not previously been observed, nor reconstructed from geological records. However, this type of lahar would probably be on a larger scale and would be destructive (Scenario 3) because of the climate condition during winter with several meters thick snowpacks at high elevation (> 3000 m).

The existing lahar hazard maps for Ontake Volcano include an assumption of potential lahars by snow melting or by heavy rainfall with a return period of 100 years following a magmatic eruption. However, potential hazards by lahars may delay in response to variable climatic conditions because thick snow packs over tephra fall deposits can prevent erosion and remobilization. Under such conditions, lahars will be large when they are associated with ROS events during a snow-melting period. Thus, the variable lahar scenarios should be considered and some of the hazard mitigation strategies for lahars should be re-accessed and revised especially at active volcanoes under a temperate climatic condition with seasonal snow cover in Japan.

Significance of clay-rich lahar deposits originating from a small phreatic eruption

The clay-rich October lahar deposits of Ontake Volcano clearly indicate that a cohesive lahar (debris flow) can be generated following a small-scale (VEI 1–2) phreatic eruption solely by rainfall without large-scale flank collapse. In addition to this 2014 example, a rain-triggered lahar after the phreatic eruption at Ontake in October 1979 (Okuda and Kashiwaya 1980) was noted to have had a texture and depositional facies similar to the October 2014 lahar (personal comm. by Hiroshi Suwa). Several other reports suggest that cohesive lahars (or muddy flows) can occur after/during phreatic eruptions, based on modern examples (Mt. Niigata-Yakeyama 1949 eruption, Sakuma and Minakami 1949; Mt. Yakedake 1962 eruption, Yamada 1962; Mt. Ruapehu 2007 eruption, Graettinger et al. 2010; Kilgour et al. 2010), implying the close relation between small-scale phreatic eruptions and the clay-rich or clay-bearing lahars. Since clay-rich lahar deposits usually are expected to derive from large-scale debris avalanche associated with flank collapse (Vallance and Scott 1997; Capra and Macías 2000; Waythomas 2006; Vallance and Iverson 2015), this interpretation of origin should be verified using geomorphological evidence: amphitheater scars on edifices, distributed hummocks in downslope deposits, and very large volumes of lahar sediments.

Mineralogical aspects (especially clay mineralogy) of clay-rich lahar deposits in association with debris avalanche often relate the origin of collapsed edifice to states of hydrothermal alteration (John et al. 2008; Detienne et al. 2017). Mineralogical and geochemical characteristics of the rain-triggered October lahar deposits at Ontake inherit information about hydrothermal alteration conditions without flank collapse. The October lahar deposits show enrichment in sulfide and sulfate minerals (Table 2), which correspond with the state of the hydrothermally altered source area. The presence of pyrophyllite in the lahar deposits, which is also one of the characteristics of the September eruption deposits, suggests the material originated from a hydrothermally altered zone at 1–2 km depth below the surface of the volcano (Minami et al. 2015), not from the edifice.

Phreatic eruptions tend to be in a smaller scale compared to magmatic eruptions, and therefore, traces of these eruptions are limited to proximal (summit) areas and are prone to be eroded soon after the deposition. Indeed, when the authors climbed up to the summit area of Ontake Volcano 12 and 22 months after the eruption (at Loc. 1289: Fig. 1a), initial ashfall deposits had been largely eroded and removed by wind, rain, and snowmelt processes. This implies the incompleteness of the geological record in documenting small phreatic eruptions. Understanding the history and recurrence intervals of phreatic

eruptions at Ontake and other volcanoes is difficult, because most of the examples are from witnessed events (Soya et al. 1980; Browne and Lawless 2001; Ohba et al. 2007; Fujinawa et al. 2008; Kilgour et al. 2010), and there must be more unknown phreatic eruptions. Although the reconstruction of phreatic events by geological records is necessary to predict and mitigate future hazards, the low preservation potential of primary eruption deposits often hampers orthodox tephrochronological methods to apply and reveal phreatic eruption histories.

On the other hand, meters-thick October lahar deposits at Ontake can be a substitute of the eruption deposits as they partially retain primary eruptive information. Similar clay-rich lahar deposits with distinctive compositions in geologic and stratigraphic records have been reported in previous studies, in relation to lahars after phreatic eruptions and/or derivation from hydrothermally altered rocks nearby eruptive sources (Hodgson et al. 2007; Kataoka et al. 2015; Minami et al. 2015). At Adatara Volcano in northeast Japan, more frequent intercalations of lahar (cohesive debris flow) deposits than those of recorded eruption deposits suggest the presence of unknown eruptions of the volcano causing the lahars (Kataoka et al. 2015). The examination of lahars at Ontake and other volcanoes in association with phreatic events implies that clay mineralogy of lahar deposits is useful to assess the presence of unknown small-scale eruptions (Cronin et al. 1997; Hodgson et al. 2007; Kataoka et al. 2015). In addition, the whole rock sulfur contents of lahar deposits are also helpful for distinguishing the syn-eruptive and/or earlier post-eruptive deposits from deposits in inter-eruptive, background sedimentation periods in geological records (Fig. 8). Some of the overbank or in-channel lahar deposits might be well preserved when river course changes or sudden aggradation occurs by subsequent eruption and lahar deposits. Therefore, clay-rich lahar deposits must be important not only for unraveling a lahar history, but also for evaluating the frequency of small-scale eruptions, which are otherwise unaccounted for. Such documentation is needed for volcanic risk assessments for populated cities/towns located at the foot/downstream of the volcanoes.

Conclusions

In association with the September 27, 2014, phreatic eruption at Ontake Volcano, one syn-eruptive lahar and two post-eruptive lahars (a rain-triggered lahar on October 5, 2014, and a ROS-triggered lahar on April 20, 2015) occurred on the southern flank of the volcano. The October lahar was triggered by the first rainstorm after the eruption having > 10 mm/h precipitation, which was the second post-eruptive storm. The lahar was a cohesive debris flow that travelled 11 km and formed very poorly sorted, massive clay-rich deposits (10–20 wt% of clay in matrix, 2.9×10^5 m^3 in volume). Most of the deposit originated from hydrothermally altered eruption material deposited near the vents, on slopes, and in valleys at the head of the catchment. The April lahar was caused by the last and largest ROS event during the snowmelt season. The lahar flow was erosional in upstream reaches, due to vigorous bank and channel erosion that exposed older pre-event deposits. The ROS-triggered lahar left hyperconcentrated flow deposits in the upstream areas and normal streamflow deposits in the lower downstream areas, suggesting flow transformation. The ROS-induced lahar deposits are fines-depleted sandy gravels and gravelly sands, derived from fluvial gravel in the river channel, terrace deposits, and October lahar deposits. The present contribution reveals that the deposits and samples of the syn-eruptive lahar in Sasaki et al. (2016) were incorrectly described as those obtained from the rain-triggered October lahar. Therefore, the volume, thickness of deposits, travel distance, sedimentary characteristics, and components of the syn-eruptive lahar as well as the October lahar in Sasaki et al. (2016) should be reconsidered and carefully cited. The recognition of the syn-eruptive lahar deposits must be difficult because they were nominal volume of deposits, and possibly, they could have been buried and eroded by the following two post-eruptive lahars.

Despite these lahars having originated from the same volcanic source within 7 months after the eruption, triggers, behavior, composition, and deposits were totally different. This is due to the proportion of water input to available sediment, controlled by rainstorm intensity, snow accumulation on slopes, rate of melting, and the availability and erodibility of volcanic deposits in valley and slopes which sometimes are covered with thick snow packs. This means that the generation, size, and types of lahars can vary with the timing of eruption, whether it happens during the pre-snow season, snow season, or rainy season. Therefore, lahar hazard assessment at Ontake as well as many other Japanese "seasonally" snow-clad volcanoes should include lahar scenario models with regard to seasonal variation. Among them, the ROS triggering of lahars is a significant process for lahars remobilizing primary deposits and posing potentially large hazards.

Good preservation potential for the clay-rich lahar deposits, like the October 2014 deposit, provides a way for geological sections to be evaluated to better reconstruct the history of phreatic eruptions. Frequent but small-scale phreatic events spread primary deposits, usually limited to proximal (summit) area, that are prone to erosion by wind, rain, and snowmelt runoff, which can pose difficulty understanding the precise eruption histories. Clay-rich lahar deposits can contain high bulk sulfur contents, sulfide/sulfate minerals, and clay minerals

diagnostic of alteration processes at depth. Such lahar deposits are often overlooked in favor of primary eruption deposits, but they may in fact preserve a better record of small-scale eruptions.

Additional file

Additional file 1. A movie, captured by a camera set at Loc. 1227 in the Akagawa River with 10 min intervals, showing rising and falling stages of the rain-on-snow-induced lahar that occurred on April 20, 2015. Records start at 5:00 a.m., April 19 and end at 9:00 a.m., April 22. The peak, which occurred at night, could not be captured.

Authors' contributions

KSK did field survey for sedimentological analysis and did contribute to write the main part of the paper and compile/interpret data. TM was engaged in river morphological survey and analyzed snowmelt water estimation. TS did field survey for petrological analyses. KK, TI, AS, and KS contributed to snow and meteorological survey for the study area. YN performed the geochemical analysis for the sedimentary samples. All authors read and approved the final manuscript.

Author details

[1] Research Institute for Natural Hazards and Disaster Recovery, Niigata University, Ikarashi 2-8050, Nishi-ku, Niigata 950-2181, Japan. [2] Department of Geology, Shinshu University, 3-1-1 Asahi, Matsumoto, Nagano 390-8621, Japan. [3] Faculty of Symbiotic Systems Science, Fukushima University, Kanayagawa 1, Fukushima 960-1296, Japan. [4] Graduate School of Engineering, Kyoto University, Katsura, Kyoto 615-8530, Japan. [5] Department of Environmental Sciences, Shinshu University, 3-1-1 Asahi, Matsumoto, Nagano 390-8621, Japan. [6] Present Address: Department of Geography and Environmental Studies, Kokushikan University, 4-28-1 Setagaya, Setagaya-ku, Tokyo 154-8514, Japan.

Acknowledgements

The authors are grateful to Kazumi Nakajima and his colleagues at the Forestry Agency, Kiso Office, for giving helpful information to do fieldwork. Koji Suzuki (Niigata University) is thanked for logistic and technical support for setting up of observation sites. Takuma Katori (Niigata University) helped us with mineral identification and XRD analysis. Analyses of XRF and laser grainsize were performed with the help of Midori Momiyama (Fukushima University) and Sanae Watabe and Keiko Yamagishi (Niigata University). Discussion with Fukashi Maeno (University of Tokyo) helped in the interpretations of original material within lahar deposits. Hiroshi Suwa (Kyoto University) is acknowledged for providing (some unpublished) information about a lahar occurred after the 1979 eruption of Ontake Volcano. The authors appreciate and acknowledge Thomas Pierson (US Geological Survey) and Christopher Gomez (Kobe University) for their thoughtful reading and constructive comments, which greatly improved the manuscript.

Competing interests

The authors declare that they have no competing interests.

Availability of data and materials

Supporting data are available on the Web site of EPS.

Consent for publication

Not applicable.

Ethics approval and consent to participate

Not applicable.

Funding

This research is fully supported by the intermural research grant: the institutional research fund at the Research Institute for Natural Hazards and Disaster Recovery, Niigata University, in FY2014 (PI: KSK, co-PI: TM) and the collaborative research grant provided by the same institution in FY2014–2015 (PI: TS, co-PI: KSK).

Appendix 1

See Table 3.

Table 3 Grainsize characteristics of ashfall, October rain-triggered lahar and April ROS-triggered lahar deposits, and pre-eruptive fluvial deposits

Sample name	Distance from source	River system	Position of sampling	Loc.	Lat. (N)	Long. (E)	Gravel (wt%)	Sand (wt%)	Silt (wt%)[1]
Pre-eruptive fluvial deposits									
On-7	10.6	Nigorigawa/Otakigawa	Pre-eruptive	950	35.803	137.482	3.6	94.9	1.5
On-11	10.6	Nigorigawa/Otakigawa	Pre-eruptive	1207	35.803	137.482	0.2	96.1	3.7
On-14	10.6	Nigorigawa/Otakigawa	Pre-eruptive	1208	35.803	137.482	0.0	96.5	3.6
On-27	4.4	Akagawa	Pre-eruptive	1191	35.853	137.464	79.3	18.3	2.4
On-33	4.1	Akagawa	Pre-eruptive	1192	35.856	137.465	39.8	58.4	1.9
On-39	4.2	Akagawa	Pre-eruptive	S114	35.854	137.464	9.1	86.6	4.4
On-40	4.2	Akagawa	Pre-mudflow event, sand layer	S114	35.854	137.464	0.0	76.4	23.6
On-43	3.0	Akagawa (upstream)	Pre-eruptive	S119	35.864	137.464	47.4	49.6	2.9
October 2014 rain-triggered lahar (cohesive debris flow) deposits									
On-13	10.6	Nigorigawa/Otakigawa	Middle-top	1207	35.803	137.482	21.1	52.9	15.6
On-18	4.8	Akagawa	Entire	1199	35.849	137.466	60.4	23.7	10.1
On-29	4.4	Akagawa	Bottom	1191	35.853	137.464	54.1	24.5	13.3
On-30	4.4	Akagawa	Top	1191	35.853	137.464	43.4	30.2	16.1
On-31	4.4	Akagawa	Middle	1191	35.853	137.464	38.6	34.0	16.6
On-34	4.1	Akagawa	Bottom	1192	35.856	137.465	36.6	36.7	15.9
On-35	4.1	Akagawa	Middle	1192	35.856	137.465	44.5	31.4	14.2
On-36	4.1	Akagawa	Top	1192	35.856	137.465	53.1	26.9	12.0
On-41	4.2	Akagawa	Top	S114	35.854	137.464	46.8	28.0	14.9

Table 3 (continued)

Sample name	Distance from source	River system	Position of sampling	Loc.	Lat. (N)	Long. (E)	Gravel (wt%)	Sand (wt%)	Silt (wt%)[1]
On-42	4.2	Akagawa	Bottom-middle	S114	35.854	137.464	38.5	32.9	16.7
On-45	3.0	Akagawa (upstream)	Bottom	S119	35.864	137.464	47.5	27.9	14.2
On-46	3.0	Akagawa (upstream)	Middle	S119	35.864	137.464	52.9	24.3	13.6
On-47	3.0	Akagawa (upstream)	Top	S119	35.864	137.464	39.8	30.7	17.9
On-50	4.7	Akagawa	Middle	1227	35.850	137.465	52.6	26.6	12.9
On-58	6.3	Nigorigawa	Middle	1232	35.837	137.469	68.1	22.7	6.0
October 2014 rain-triggered lahar (cohesive debris flow) deposits: sole fine layer									
On-12	10.6	Nigorigawa/Otakigawa	Sole layer	1207	35.803	137.482	0.0	47.4	33.4
On-28	4.4	Akagawa	Sole layer	1191	35.853	137.464	0.0	40.3	35.3
April 2015 rain-on-snow-triggered lahar deposits									
On-15	10.6	Nigorigawa/Otakigawa	Lower	1208	35.803	137.482	0.0	96.2	3.8
On-16	10.6	Nigorigawa/Otakigawa	Upper	1208	35.803	137.482	0.0	95.7	4.3
On-19	4.8	Akagawa	Over bank (peak flow) facies	1199	35.849	137.466	80.7	18.1	1.3
On-20	4.8	Akagawa	Flow waning stage	1199	35.849	137.466	40.9	57.4	1.7
On-48	10.6	Nigorigawa/Otakigawa	Surface (bar top)	1206	35.803	137.481	0.0	94.1	5.9
On-51	4.7	Akagawa	Top	1227	35.850	137.465	35.5	61.6	2.9
On-52	4.7	Akagawa	Middle	1227	35.850	137.465	67.2	30.3	2.5
On-53	4.7	Akagawa	Bottom	1227	35.850	137.465	54.0	43.6	2.4
On-54	7.3	Nigorigawa/Denjogawa	Upper	1228	35.828	137.471	74.5	25.1	0.4
On-55	7.3	Nigorigawa/Denjogawa	Lower	1228	35.828	137.471	24.0	75.2	0.8
On-56	7.3	Nigorigawa/Denjogawa	Top	1229	35.828	137.471	1.6	97.1	1.3
On-57	7.3	Nigorigawa/Denjogawa	Middle	1229	35.828	137.471	18.0	81.3	0.7
April 2015 rain-on-snow-triggered lahar deposits (mud drape)									
On-21	4.8	Akagawa	Entire	1199	35.849	137.466	0.0	28.0	48.2
On-32	4.4	Akagawa	Entire	1191	35.853	137.464	0.0	22.1	46.9
September 2014 Primary deposits									
On-64	–	Nearby the summit	Ashfall lower	1289	35.895	137.488	0.0	12.0	52.0
On-65	–	Nearby the summit	Ashfall upper (aggregates)	1289	35.895	137.488	0.0	15.2	50.1
On-66	–	Nearby the summit	Ashfall uppermost (aggregates+reworked)	1289	35.895	137.488	0.0	19.5	48.9
On-44	3.0	Akagawa (upstream)	Ashcloud deposits?	S119	35.864	137.464	0.0	18.9	64.3
Shirakawa River deposits									
On-22	–	Shirakawa	Pre-eruptive fluvial deposits	1202	35.854	137.462	3.8	94.0	2.1
On-23	–	Shirakawa	Post-eruptive reworked ash	1202	35.854	137.462	0.0	39.7	48.0
On-24	–	Shirakawa	October 2014 runoff?	1202	35.854	137.462	0.0	51.2	48.7
On-25	–	Shirakawa	October 2014 runoff?	1202	35.854	137.462	0.0	72.0	28.0
On-26	–	Shirakawa	Rain-on-snow runoff/entire	1202	35.854	137.462	0.2	86.3	13.5

Sample name	Clay (wt%)	Clay in matrix (wt%)[2]	Median grainsize Mdφ[3]	Mean grainsize Mz	Sorting σ_I	Skewness Sk_I	Kurtosis K_G	Method[4]
Pre-eruptive fluvial deposits								
On-7			2.02	1.96	1.04	−0.15	1.26	a
On-11			2.28	2.26	0.85	0.03	1.09	a
On-14			2.28	2.25	0.93	−0.02	1.08	a
On-27			−4.28	−3.04	2.33	0.80	1.15	a
On-33			−0.57	−0.68	1.79	−0.04	1.05	a
On-39			1.10	1.10	1.60	−0.01	1.16	a
On-40			3.26	3.40	1.03	0.24	1.10	a
On-43			−0.89	−0.84	1.60	0.17	1.01	a

Table 3 (continued)

Sample name	Clay (wt%)	Clay in matrix (wt%)[2]	Median grainsize Mdφ[3]	Mean grainsize Mz	Sorting σ_I	Skewness Sk_I	Kurtosis K_G	Method[4]
October 2014 rain-triggered lahar (cohesive debris flow) deposits								
On-13	10.5	13.3	0.87	2.10	3.76	0.46	0.93	b
On-18	5.8	14.7	− 2.52	− 1.05	4.14	0.58	0.90	b
On-29	8.1	17.6	− 1.84	− 0.23	4.29	0.69	0.57	b
On-30	10.4	18.4	0.04	0.82	4.91	0.26	0.71	b
On-31	10.8	17.6	0.60	1.28	4.73	0.22	0.77	b
On-34	10.8	17.0	0.54	1.27	4.68	0.24	0.82	b
On-35	9.9	17.9	− 0.21	0.41	5.02	0.25	0.67	b
On-36	8.0	17.1	− 1.55	− 0.35	4.73	0.42	0.74	b
On-41	10.3	19.3	− 0.51	0.38	5.07	0.30	0.65	b
On-42	12.0	19.4	0.59	1.29	4.91	0.23	0.72	b
On-45	10.4	19.9	− 0.59	0.65	4.43	0.54	0.53	b
On-46	9.2	19.6	− 1.47	0.15	4.33	0.67	0.55	b
On-47	11.7	19.4	0.50	1.27	4.87	0.24	0.69	b
On-50	8.0	16.8	− 1.49	− 0.23	4.48	0.53	0.70	b
On-58	3.3	10.2	− 3.28	− 2.10	3.33	0.64	1.06	b
October 2014 rain-triggered lahar (cohesive debris flow) deposits: sole fine layer								
On-12	19.3	19.3	4.29	4.74	3.18	0.19	0.78	c
On-28	24.3	24.3	5.40	5.38	3.08	0.02	0.70	c
April 2015 rain-on-snow-triggered lahar deposits								
On-15			2.51	2.52	0.78	0.03	1.17	a
On-16			2.38	2.36	0.76	0.06	1.22	a
On-19			− 3.17	− 2.92	1.87	0.52	0.73	a
On-20			− 0.50	− 0.45	2.04	0.07	0.90	a
On-48			2.14	2.16	1.08	0.05	1.11	a
On-51			− 0.26	− 0.39	1.93	− 0.05	1.00	a
On-52			− 2.51	− 1.99	2.56	0.32	0.82	a
On-53			− 1.17	− 1.04	1.72	0.18	1.10	a
On-54			− 3.87	− 2.81	2.07	0.77	0.58	a
On-55			− 0.01	− 0.18	1.63	− 0.25	1.44	a
On-56			1.26	1.21	0.89	− 0.04	1.20	a
On-57			0.25	0.16	1.30	− 0.13	1.13	a
April 2015 rain-on-snow-triggered lahar deposits (mud drape)								
On-21	23.8	23.8	5.52	5.85	2.50	0.20	0.77	c
On-32	31.0	31.0	6.37	6.36	2.59	0.02	0.76	c
September 2014 primary deposits								
On-64	36.0	36.0	7.10	6.92	2.31	− 0.09	0.84	c
On-65	34.7	34.7	6.99	6.78	2.47	− 0.11	0.86	c
On-66	31.6	31.6	6.70	6.43	2.65	− 0.13	0.89	c
On-44	16.7	16.7	5.06	5.69	2.08	0.46	1.10	c
Shirakawa River deposits								
On-22			1.27	1.28	1.26	0.01	1.06	a
On-23	12.3	12.3	4.44	4.78	2.35	0.28	1.32	c
On-24			3.97	4.21	0.95	0.32	0.79	a
On-25			3.41	3.54	1.03	0.21	1.04	a
On-26			2.43	2.50	1.39	0.13	1.23	a

[1] Silt indicates particles of < 0.063 mm when manual sieving methods

[2] Clay/(sand + silt + clay)

[3] Grain characters based on Folk (1974)

[4] Methods: a) dry sieving, b) wet sieving and laser analyzer, and c) laser analyzer

Appendix 2

See Table 4.

Table 4 Results of XRF (bulk chemistry) of ashfall, rain-triggered lahar and ROS-triggered lahar deposits, and pre-eruptive fluvial deposits

Lithology	Sample name	SiO_2 (wt%)	TiO_2	Al_2O_3	$Fe_2O_3^a$	MnO	MgO	CaO	Na_2O	K_2O	P_2O_5	SO_3^b	Others	Total
FP method for sediments analyzed by Rigaku RIX 1000														
September 2014 primary deposits														
Ashfall	On-1	57.03	0.87	16.46	5.62	0.03	0.53	1.37	1.11	2.12	0.30	14.29	0.25	100.00
Ash could deposits	On-44	56.13	0.61	14.65	5.31	0.04	1.12	4.18	1.29	1.90	0.36	14.23	0.19	100.00
October 2014 rain-triggered lahar (Cohesive debris flow) deposits														
Muddy	On-2	56.77	0.95	15.24	6.12	0.05	0.91	3.16	1.07	2.27	0.37	12.90	0.19	100.00
Muddy	On-3	55.40	1.03	13.68	7.12	0.06	0.89	3.62	1.72	2.07	0.33	13.91	0.18	100.00
Muddy	On-4	58.66	0.93	15.45	5.49	0.05	0.95	3.20	1.17	2.21	0.36	11.34	0.18	100.00
Muddy	On-5	59.62	0.97	13.38	6.24	0.04	0.64	2.95	1.11	1.92	0.29	12.66	0.18	100.00
Muddy	On-6	57.80	1.07	14.46	6.80	0.08	1.20	3.65	1.94	2.16	0.32	10.34	0.18	100.00
Muddy	On-13	57.89	0.88	15.36	5.94	0.06	0.99	3.43	1.38	2.31	0.29	11.26	0.21	100.00
Muddy	On-18	58.16	0.96	15.45	5.43	0.05	0.88	2.68	1.49	2.25	0.36	12.11	0.18	100.00
Muddy	On-34	57.57	0.87	15.98	5.73	0.05	0.97	3.15	1.47	2.20	0.36	11.49	0.16	100.00
Muddy	On-45	56.90	0.80	15.50	5.51	0.06	1.03	3.33	1.37	2.10	0.32	12.79	0.28	100.00
April 2015 rain-on-snow-triggered lahar deposits														
Sandy	On-16	61.05	1.00	15.66	5.90	0.09	1.10	4.29	1.82	2.41	0.29	6.21	0.18	100.00
Sand-gravel	On-19	65.65	0.91	15.53	4.55	0.07	0.67	3.32	1.76	2.73	0.33	4.31	0.17	100.00
Sandy	On-26	64.92	0.64	16.67	4.72	0.11	1.00	5.05	2.89	2.95	0.29	0.62	0.14	100.00
Sand-gravel	On-51	60.26	1.06	14.80	5.85	0.06	1.00	3.20	2.07	2.58	0.28	8.65	0.19	100.00
April 2015 rain-on-snow-triggered lahar deposits (mud drape)														
Muddy	On-21	57.75	0.77	18.31	5.81	0.03	1.09	1.58	1.10	2.20	0.53	10.69	0.15	100.00
Pre-eruptive fluvial deposits														
Sandy	On-7	61.90	1.14	15.80	6.85	0.14	1.31	5.25	2.44	2.60	0.36	2.08	0.15	100.00
Sandy	On-11	63.89	0.97	16.07	5.87	0.11	1.08	4.99	2.28	2.63	0.34	1.58	0.20	100.00
Sandy	On-17	65.68	0.78	15.45	5.27	0.11	0.97	4.15	2.38	3.03	0.37	1.65	0.16	100.00
Sandy	On-22	66.35	0.67	15.68	4.73	0.10	0.98	4.71	2.97	3.14	0.27	0.27	0.14	100.00
Sand-gravel	On-33	66.57	0.99	15.34	4.44	0.08	0.90	3.80	1.82	2.75	0.28	2.83	0.20	100.00
Sand-gravel	On-43	64.38	1.01	15.67	4.90	0.08	0.99	4.01	1.65	2.63	0.36	4.11	0.21	100.00
Shirakawa deposits														
Muddy	On-23	61.81	0.70	15.06	5.18	0.05	0.98	2.97	1.55	2.34	0.27	8.94	0.16	100.00
Sandy	On-24	60.73	0.78	16.08	5.36	0.07	0.99	3.92	2.38	2.45	0.43	6.66	0.16	100.00

Sample name	As (ppm)	Ba	Co	Cr	Cu	Nb	Ni	Pb	Sr	V	Zn	Total
Calibration method for sediments analyzed by Rigaku RIX 2000												
September 2014 primary deposits												
On-1	24	475	16	37	13	8	10	13	528	198	72	1654
On-44	15	495	13	36	15	8	8	16	551	127	100	1652
October 2014 rain-triggered lahar (Cohesive debris flow) deposits												
On-2	16	462	17	36	12	8	10	10	540	200	73	1636
On-3	15	487	16	39	13	9	8	12	546	195	85	1685
On-4	12	457	14	62	12	8	13	12	545	190	72	1659
On-5	16	425	17	36	13	9	11	12	531	184	75	1591
On-6	14	482	17	36	11	10	10	10	557	202	83	1690
On-13	14	479	15	34	12	9	9	11	533	182	70	1627

Table 4 (continued)

Sample name	As (ppm)	Ba	Co	Cr	Cu	Nb	Ni	Pb	Sr	V	Zn	Total
On-18	13	463	13	34	10	9	7	12	532	193	55	1614
On-34	15	456	12	33	12	9	8	13	547	188	66	1635
On-45	16	473	15	35	14	9	12	11	546	187	78	1645
April 2015 rain-on-snow-triggered lahar deposits												
On-16	10	468	13	34	10	10	11	11	590	185	75	1669
On-19	8	529	8	28	9	9	8	13	529	165	61	1659
On-26	3	554	9	27	8	9	8	13	603	119	77	1697
On-51	12	488	12	34	12	9	10	11	550	202	59	1673
April 2015 rain-on-snow-triggered lahar deposits (mud drape)												
On-21	21	508	13	33	13	8	8	16	572	195	68	1727
Pre-eruptive fluvial deposits												
On-7	6	489	13	35	9	11	11	10	564	213	96	1732
On-11	5	511	10	28	9	9	9	12	597	182	77	1712
On-17	5	566	9	28	7	10	10	12	533	155	75	1704
On-22	3	591	11	26	7	11	10	14	546	122	82	1731
On-33	7	520	9	30	6	10	8	11	507	188	65	1663
On-43	8	496	10	31	9	10	10	10	546	200	67	1668
Shirakawa deposits												
On-23	10	503	8	27	9	8	6	13	527	110	54	1529
On-24	9	519	9	29	11	8	8	13	579	143	66	1655

[a] Total iron oxide as Fe_2O_3; [b]total sulfur as SO_3

Publisher's Note

Received: 27 February 2018 Accepted: 12 June 2018
Published online: 05 July 2018

References

Allen JRL (1982) Sedimentary structures: their character and physical basis, volume I. Dev Sedimentol 30:1–593

Baas JH, Best JL, Peakall J, Wang M (2009) A phase diagram for turbulent transitional and laminar clay suspension flows. J Sediment Res 79:162–183

Baas JH, Best JL, Peakall J (2011) Depositional processes, bedform development and hybrid flows in rapidly decelerated cohesive (mud-sand) sediment flows. Sedimentology 58:1953–1987

Browne PRL, Lawless JV (2001) Characteristics of hydrothermal eruptions, with examples from New Zealand and elsewhere. Earth Sci Rev 52:299–331

Capra L, Macías JL (2000) Pleistocene cohesive debris flows at Nevado de Toluca Volcano, central Mexico. J Volcanol Geotherm Res 102:149–168

Cronin SJ, Neall VE, Lecointre JA, Palmer AS (1997) Changes in Whangaehu River lahar characteristics during the 1995 eruption sequence, Ruapehu volcano, New Zealand. J Volcanol Geotherm Res 76:47–61

Detienne M, Delmelle P, Guevara A, Samaniego P, Opfergelt S, Mothes PA (2017) Contrasting origin of two clay-rich debris flows at Cyambe Volcanic Complex Ecuador. Bull Volcanol 79:27–40

DeWalle DR, Rango A (2008) Principles of snow hydrology. Cambridge University Press, Cambridge

Endo K, Sumita M, Machida M, Furuichi M (1989) The 1984 collapse and debris avalanche deposits of Ontake Volcano, central Japan. In: Latter JH (ed) Volcanic hazards, IAVCEI proceedings in volcanology. Springer, Berlin, pp 210–229

Fisher RV, Schmincke H-U (1984) Pyroclastic rocks. Springer, Berlin

Folk RL (1974) Petrology of sedimentary rocks. Hemphill Publishing Co., Austin, TX, p 182

Fujinawa A, Ban M, Ohba T, Kontani K, Miura K (2008) Characterization of low-temperature pyroclastic surges that occurred in the northeastern Japan arc during the late 19th century. J Volcanol Geotherm Res 178:113–130

Goldman SJ, Jackson K, Bursztynsky TA (1986) Erosion and sediment control handbook. McGraw-Hill, New York

Graettinger AH, Manville V, Briggs RM (2010) Depositional record of historic lahars in the Upper Whangaehu Valley, Mt. Ruapehu, New Zealand: implications for trigger mechanisms, flow dynamics, and lahar hazards. Bull Volcanol 72:279–296

Hampton MA (1975) Competence of fine-grained debris flows. J Sediment Petrol 45:834–844

Harpel CJ, de Silva S, Salas G (2013) Comment on: "Cobeñas, G., Thouret, J.-C., Bonadonna, C., Boivin, P., 2012. The c.2030 yr BP Plinian eruption of El Misti volcano, Peru: eruption dynamics and hazard implications. J Volcanol Geotherm Res 241–242, 105–120". J Volcanol Geotherm Res 265:94–101

Hayashi S, Kitahara O, Kusano S, Watari M, Nagai Y, Kunitomo M, Ishizuoka T, Fujimura N, Shimizu T (2015) Emergency survey and countermeasure for disaster due to eruption of Mt. Ontake on September 2014. J Jpn Soc Eros Control Eng 67:86–91 **(in Japanese)**

Hodgson KA, Lecontre JA, Neall VE (2007) Onetapu Formation: the last 2000 yr of laharic activity at Ruapehu volcano, New Zealand. N Z J Geol Geophys 50:81–99

John DA, Sisson TW, Breit GN, Rye RO, Vallance JW (2008) Characteristics, extent and origin of hydrothermal alteration at Mount Rainier Volcano, Cascades Arc, USA: implications for debris-flow hazards and mineral deposits. J Volcanol Geotherm Res 175:289–314

Kaneko T, Maeno F, Nakada S (2016) 2014 Mount Ontake eruption: characteristics of the phreatic eruption as inferred from aerial observations. Earth Planets Space 68:72–82. https://doi.org/10.1186/s40623-016-0452-y

Kataoka KS, Manville V, Nakajo T, Urabe A (2009) Impacts of explosive volcanism on distal alluvial sedimentation: examples from the Pliocene–Holocene volcaniclastic successions of Japan. Sediment Geol 220:306–317

Kataoka KS, Kamino N, Nagahashi Y, Kimura K (2015) Stratigraphy, chronology and depositional processes of lahar deposits in the Sukawa River System, Adatara volcano, northeast Japan. Bull Volcanol Soc Jpn 60:461–475 **(in Japanese with English abstract)**

Kattelmann R (1985) Macropores in snowpacks of Sierra Nevada. Ann Glaciol 6:272–273

Kattelmann R (1997) Flooding from rain-on-snow events in the Sierra Nevada. IAHS Publ 239:59–65

Kilgour G, Manville V, Della Pasqua F, Graettinger A, Hodgson KA, Jolly GE (2010) The 25 September 2007 eruption of Mount Ruapehu, New Zealand: directed ballistics, surtseyan jets, and ice-slurry lahars. J Volcanol Geotherm Res 191:1–14

Maeno F, Nakada S, Oikawa T, Yoshimoto M, Komori J, Ishizuka Y, Takeshita Y, Shimano T, Kaneko T, Nagai M (2016) Reconstruction of a phreatic eruption on 27 September 2014 at Ontake volcano, central Japan, based on proximal pyroclastic density current and fallout deposits. Earth Planets Space 68:82–101. https://doi.org/10.1186/s40623-016-0449-6

Major JJ, Newhall CG (1989) Snow and ice perturbation during historical volcanic eruptions and the formation of lahars and floods—a global review. Bull Volcanol 52:1–27

Manville V, Hodgson KA, Houghton BF, Keys JRH, White JDL (2000) Tephra, snow and water: complex sedimentary responses at an active snow-capped stratovolcano, Ruapehu, New Zealand. Bull Volcanol 62:278–293

Marks D, Kimball J, Tingey D, Link T (1998) The sensitivity of snowmelt processes to climate conditions and forest cover during rain-on-snow: a case study of the 1996 Pacific Northwest flood. Hydrol Process 12:1569–1587

Marks D, Link T, Winstral A, Garen D (2001) Simulating snowmelt processes during rain-on-snow over a semi-arid mountain basin. Ann Glaciol 32:195–202

Matsuda T, Ariyama T (1985) Debris avalanche deposits of the Ontake Volcano, caused by the 1984 western Nagano Prefecture earthquake—on the debris-spray zone. Bull Earthq Res Inst 60:281–316

Minami Y, Ohba T, Hayashi S, Kataoka KS (2015) Depositional processes and temporal component-change of lahar deposits at the northern foot of Chokai volcano, NE Japan. Bull Volcanol Soc Jpn 60:1–16 **(in Japanese with English abstract)**

Minami Y, Imura T, Hayashi S, Ohba T (2016) Mineralogical study on volcanic ash of the eruption on September 27, 2014 at Ontake volcano, central Japan: correlation with porphyry copper systems. Earth Planets Space 68:67–77. https://doi.org/10.1186/s40623-016-0440-2

Nagahashi Y, Nakazawa N (2016) Application of non-destructive and sequential analyses of chemical composition using by scanning X-ray analytical microscope (SXAM): a case study of Lake Inawashiro-ko sediment core. Quat Res 55:223–236 **(in Japanese with English abstract)**

Newhall CG, Punongbayan RS (eds) (1996) Fire and mud—eruptions and lahars of Mount Pinatubo, Philippines. Philippine Institute of Volcanology and Seismology and the University of Washington Press, Seattle

Nomura Y, Kosugi K, Mizuyama T (2003) Physical properties of volcanic ash deposits in Miyakejima, Mt. Usu and Sakurajima—analysis of physical properties of ash deposits in relation to mudflow occurrences. J Jpn Soc Eros Control Eng 55:3–12 **(in Japanese with English abstract)**

Ohba T, Kitade Y (2005) Subvolcanic hydrothermal systems: implication from hydrothermal minerals in hydrovolcanic ash. J Volcanol Geotherm Res 145:249–262

Ohba T, Taniguchi H, Miyamoto T, Hayashi S, Hasenaka T (2007) Mud plumbing system of an isolated phreatic eruption at Akita Yakeyama volcano, northern Honshu, Japan. J Volcanol Geotherm Res 161:35–46

Oikawa T, Suzuki Y, Chiba T (2014) Eruption history and 2014 eruption of Ontake volcano. Kagaku 84:1218–1225 **(in Japanese)**

Oikawa T, Yamaoka K, Yoshimoto M, Nakada S, Takeshita Y, Maeno F, Ishizuka Y, Komori J, Shimano T, Nakano S (2015) The 2014 eruption of Ontake Volcano, central Japan. Bull Volcanol Soc Jpn 60:411–415 **(in Japanese)**

Oikawa T, Yoshimoto M, Nakada S, Maeno F, Komori J, Shimano T, Takeshita Y, Ishizuka Y, Ishimine Y (2016) Reconstruction of the 2014 eruption sequence of Ontake Volcano from recorded images and interviews. Earth Planets Space 68:79–91. https://doi.org/10.1186/s40623-016-0458-5

Okuda S, Kashiwaya K (1980) Catchment geomorphological features and possibility of lahar generation induced by ashfall around Ontake Volcano (Ontakesan-shuhenkeiryuikino-chikeitokuseikaramita-kouhainiyoru-deiryuhasseino-kanouseinitsuite). In: Aoki H (ed) Integrated researches on eruptive activities and hazards of Kiso-Ontakesan volcano (Kiso-Ontakesan-funkakatsudo-oyobi-saigai-no-sougouteki-chousaken-kyu), Uji, Kyoto, pp 109–114

Pierson TC (2005) Hyperconcentrated flow—transitional process between water flow and debris flow. In: Jacob M, Hungr O (eds) Debris-flow hazards and related phenomena. Springer, Chichester, pp 159–202

Pierson TC, Major JJ (2014) Hydrogeomorphic effects of explosive volcanic eruptions on drainage basins. Annu Rev Earth Planet Sci 42:469–507

Pierson TC, Janda RJ, Thouret J-C, Borrero CA (1990) Perturbation and melting of snow and ice by the 13 November 1985 eruption of Nevado del Ruiz, Colombia, and consequent mobilization, flow and deposition of lahars. J Volcanol Geotherm Res 41:17–66

Pierson TC, Major JJ, Amigo Á, Moreno H (2013) Acute sedimentation response to rainfall following the explosive phase of the 2008–2009 eruption of Chaitén volcano, Chile. Bull Volcanol 75:723–741

Pradhanang SM, Frei A, Zion M, Schneiderman EM, Steenhuis TS, Pierson D (2013) Rain-on-snow runoff events in New York. Hydrol Process 27:3035–3049

Pringle P, Scott K (2001) Postglacial influence of volcanism on the landscape and environmental history of the Puget Lowland, Washington—a review of geologic literature and recent discoveries, with emphasis on the landscape disturbances associated with lahars, lahar runouts, and associated flooding. In: Washington State Puget Sound Water Quality Action Team (ed) Puget Sound Research 2001, Proceedings. Olympia Washington, 23 p

Sakuma S, Minakami T (1949) Minor activity of Volcano Yake-yama in 1949. Bull Earthq Res Inst 27:117–121

Sasaki T, Chiba T, Kishimoto H, Naruke S (2016) Characteristics of the syneruptive-spouted type lahar generated by the September 2014 eruption of Mount Ontake, Japan. Earth Planets Space 68:141–151. https://doi.org/10.1186/s40623-016-0516-z

Sato E, Shimbori T, Fukui K, Ishii K, Takagi A (2016) The eruption could echo from Mt. Ontake on September 27, 2014 observed by weather radar network. Report of Japanese Coordinating Committee for the prediction of volcanic eruption, vol 119, pp 76–81

Scott KM, Vallance JW, Pringle PT (1995) Sedimentology, behavior, and hazards of debris flows at Mount Rainier, Washington. U.S. Geol Surv Professional Paper 1547, 56 p

Smith GA (1986) Coarse-grained nonmarine volcaniclastic sediment: terminology and depositional process. Geol Soc Am Bull 97:1–10

Smith GA (1991) Facies sequences and geometries in continental volcaniclastic sequences. In: Fisher RV, Smith GA (eds) Sedimentation in volcanic settings: SEPM (Society for Sedimentary Geology) Special Publication, vol 45, pp 109–121

Smith GA, Lowe DR (1991) Lahars: volcano-hydrologic events and deposition in the debris flow—hyperconcentrated flow continuum. In: Fisher RV, Smith GA (eds) Sedimentation in volcanic settings: SEPM (Society for Sedimentary Geology) Special Publication, vol 45, pp 59–70

Sobieszczyk S, Uhrich MA, Piatt DR, Bragg HM (2008) Analysis of geomorphic and hydrologic characteristics of Mount Jefferson debris flow, Oregon, November 6, 2006. USGS Scientific Investigations Report 2008–5204, 18 p

Sohn YK, Rhee CW, Kim BC (1999) Debris flow and hyperconcentrated flood-flow deposits in an alluvial fan, northwestern part of the Cretaceous Yongdong basin, central Korea. J Geol 107:111–132

Soya T, Kondo Y, Shimosaka K (1980) Mt. Ontake-san 1979 eruption (Ontake-san 1979 nen funka). Chishitsu News 306:6–13 **(in Japanese)**

Sui J, Koehler G (2001) Rain-on-snow induced flood events in Southern Germany. J Hydrol 252:205–220

Takarada S, Oikawa T, Furukawa R, Hoshizumi H, Itoh J, Geshi N, Miyagi I (2016) Estimation of total discharged mass from the phreatic eruption of Ontake Volcano, central Japan, on September 27, 2014. Earth Planets Space 68:138–146. https://doi.org/10.1186/s40623-016-0511-4

Takase T, Nagahashi Y (2007) Determination of major and trace elements in rock samples by X-ray fluorescence spectrometry—comparison with a glass beads method and a powder pellets method. J Center Reg Aff Fukushima Univ 19:32–47 **(in Japanese with English abstract)**

Vallance JW, Iverson RM (2015) Lahars and their deposits. In: Sigurdsson H, Houghton B, Rymer H, Stix J, McNutt S (eds) Encyclopedia of volcanoes, 2nd edn. Elsevier, Amsterdam, pp 649–664

Vallance JW, Scott KM (1997) The Osceola Mudflow from Mount Rainier: sedimentology and hazard implications of a huge-clay-rich debris flow. Geol Soc Am Bull 109:143–163

Waythomas CF (2006) Mid-holocene sector collapse at Mount Spurr Volcano, South-Central Alaska. Studies by the U.S. Geological Survey in Alaska, 2006 U.S. Geol Surv Professional Paper, vol 1739-C, pp 1–15
Waythomas CF (2014) Water, ice and mud: lahars and lahar hazards at ice- and snow-clad volcanoes. Geol Today 30:34–39
Wischmeier WH, Smith DD (1978) Predicting rainfall erosion losses—a guide to conservation planning. US Department of Agriculture, Washington, DC
Yamada T (1962) Report of the 1962 activity of Yakedake Volcano, central Japan. J Fac Lib Arts Sci Shinshu Univ Part 2 Nat Sci 12:47–81
Yamamoto T (2014) The pyroclastic density currents generated by the September 27, 2014 phreatic eruption of Ontake Volcano, Japan. Bull Geol Surv Jpn 65:117–127